University of Groningen

Optical preparation and detection of spin coherence in molecules and crystal defects

Lof, Gerrit

DOI:
10.33612/diss.109567350

IMPORTANT NOTE: You are advised to consult the publisher's version (publisher's PDF) if you wish to cite from it. Please check the document version below.

Document Version
Publisher's PDF, also known as Version of record

Publication date:
2020

Link to publication in University of Groningen/UMCG research database

Citation for published version (APA):
Lof, G. (2020). *Optical preparation and detection of spin coherence in molecules and crystal defects*. [Thesis fully internal (DIV), University of Groningen]. University of Groningen. https://doi.org/10.33612/diss.109567350

Copyright
Other than for strictly personal use, it is not permitted to download or to forward/distribute the text or part of it without the consent of the author(s) and/or copyright holder(s), unless the work is under an open content license (like Creative Commons).

The publication may also be distributed here under the terms of Article 25fa of the Dutch Copyright Act, indicated by the “Taverne” license. More information can be found on the University of Groningen website: https://www.rug.nl/library/open-access/self-archiving-pure/taverne-amendment.

Take-down policy
If you believe that this document breaches copyright please contact us providing details, and we will remove access to the work immediately and investigate your claim.

Downloaded from the University of Groningen/UMCG research database (Pure): http://www.rug.nl/research/portal. For technical reasons the number of authors shown on this cover page is limited to 10 maximum.

Download date: 06-08-2025

Chapter 3

Proposal for time-resolved optical preparation and detection of triplet-exciton spin coherence in organic molecules

Abstract

Changes in optical polarization upon light-matter interaction can probe chirality, magnetization and non-equilibrium spin orientation of matter, and this underlies fundamental optical phenomena such as circular dichroism and Faraday and Kerr rotation. With fast optical pulses electronic spin dynamics in materials can be initiated and detected in a time-resolved manner. This has been applied to material systems with high order and symmetry (giving distinct optical selection rules), such as clouds of alkali atoms and direct-band-gap semiconductor systems, also in relation to proposals for spintronic and quantum technologies. For material systems with lower symmetry, however, the potential of these phenomena for studying and controlling spin is not well established. We present here how pulsed optical techniques give access to preparing and detecting the dynamics of triplet spin coherence in a broad range of (metal-)organic molecules that have significant spin-orbit coupling. We establish how the time-resolved Faraday rotation technique can prepare and detect spin coherence in flat molecules with C_{2v} symmetry, and extrapolate that the effects persist upon deviations from this ideal case, and upon ensemble averaging over fully randomized molecular orientations. For assessing the strength and feasibility of the effects in reality, we present detailed theoretical-chemistry calculations.

3.1 Introduction

Organic molecules are increasingly used for opto-electronic devices, because of their chemical tunability, low-cost, and ease of processing. In such devices, the ratio of singlet to triplet excitons can be an important performance parameter[39]. Moreover, because of the many interesting spin-related phenomena discovered in organic semiconductors and molecules[40–45], further exploration of spintronic applications in these materials is of interest. Both for organic opto-electronics and spintronics, being able to control and probe triplet-exciton spin coherence will be of great value for better material studies and improving the functionalities. A handle for this may rely on the optical polarization of the interacting light. Correlations between electronic spin states and optical polarization are well established for inorganic semiconductors with strong spin-orbit coupling (SOC)[9], and a particular example for using such correlations is the Time-Resolved Faraday Rotation (TRFR) technique[12, 13, 46]. This is a pump-probe technique based on measuring the polarization rotation (optical rotation angle) of a probe pulse upon transmission through a sample, as a measure for the (precessing) spin orientation induced by a pump pulse. The oscillation of the polarization rotation as a function of the delay time between pump and probe then directly reflects coherent spin dynamics. The aim of the theoretical work in this chapter is to study how this pump-probe technique also allows for optical control and probing of coherent triplet-exciton spin dynamics in organic molecules.

3.2 Theoretical proof of principle for a molecular TRFR experiment

To realize a molecular TRFR experiment (Fig. 3.1), we suggest to use an ultrashort polarized pump pulse that excites a molecular system from the singlet ground state into a coherent superposition of two sublevels of the lowest triplet excited state (Fig. 3.2a), for the zero-phonon optical transition. This energy level scheme differs from the most common TRFR scenario, which focuses on electron spin coherence (with spin $S = 1/2$) in inorganic semiconductors[12, 13]. For

---

This chapter is based on Ref. 2 on p. 177.

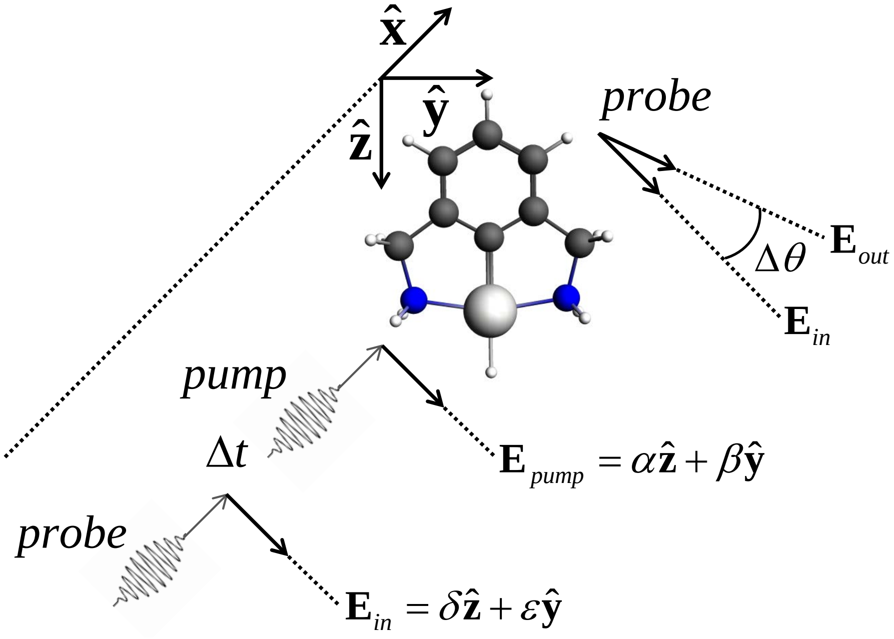

Figure 3.1: Schematic of a molecular Time-Resolved Faraday Rotation (TRFR) experiment. The pump and probe pulse propagate in the x-direction, whereas the molecule lies in the yz-plane. Depending on the state of the molecule, the probe pulse experiences optical rotation upon transmission, where the optical Faraday rotation angle $\Delta\theta$ (in the yz-plane) is a measure for the spin orientation induced by the pump pulse. Coherent spin dynamics occurs along the x-axis and is revealed by varying the delay time between pump and probe, involving an oscillation of $\Delta\theta$. In view of this work, the metal-organic molecule (2,6-bis(aminomethyl)phenyl)(hydrido)platinum is depicted, which is referred to as $\mathrm{PtN_2C_8H_{12}}$. This molecule has C_{2v} symmetry. The Jones vectors $\mathbf{E}$ with corresponding (in general complex) prefactors (α, β, δ and ϵ) are in general not normalized, unless representing polarizations (i.e. normalized electric vectors which we denote with a hat, in which case we call the prefactors polarization parameters).

these systems optical transitions can be described as excitations of single electrons, from valence-band to conduction-band states. For the relevant electrons in chemically stable organic molecules the typical situation is very different: the ground state has two localized electrons in a spin singlet $S = 0$ configuration. Without SOC effects, optical transitions are only allowed to excited states that are also singlet states. Spin coherence can be carried out by excited states with the electrons in a triplet spin $S = 1$ configuration, and these states have energies that are typically ∼200 meV lower in energy than their singlet equivalents. Optical transitions directly into the triplet excited states are only possible when

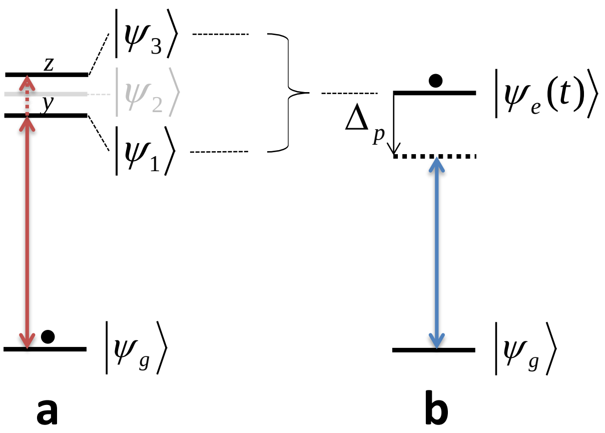

Figure 3.2: Energy level scheme and laser (de)tuning for the pump and probe pulse in a molecular Time-Resolved Faraday Rotation (TRFR) experiment. **a**, For $PtN_2C_8H_{12}$ all three (x, y, z, as defined in Fig. 3.1) components of $\langle\psi_2|\,\mathbf{r}\,|\psi_g\rangle$ are zero, wherefore we neglect $|\psi_2\rangle$. When the pump pulse (red arrow) arrives at $t = 0$, only $|\psi_g\rangle$ is populated, as indicated with the dot. Full absorption of a photon out of a short (thus spectrally broad) optical pump pulse polarized in both the y and z-direction induces a superposition of $|\psi_1\rangle$ and $|\psi_3\rangle$. **b**, Directly after excitation with the pump, $|\psi_e(t)\rangle$ (being a superposition of $|\psi_1\rangle$ and $|\psi_3\rangle$) is populated, as indicated with the dot. A linearly polarized probe pulse (blue arrow) with detuning Δ_p experiences a polarization rotation $\Delta\theta$, which oscillates as a function of the delay time Δt. This oscillation is a measure for the coherent spin dynamics $\langle\mathbf{J}\rangle(t)$, related to the evolution $|\psi_e(t)\rangle$.

the system has significant SOC, with more oscillator strength for the transitions as the SOC strength increases. Typical molecular systems with large SOC are metal-organic complexes containing a heavy metal atom[47, 48], and molecules with strong curvature at carbon-carbon bonds[49]. Such molecules are particularly used in organic light-emitting diodes (OLEDs) for efficient triplet-exciton harvesting.

For our analysis we will assume that the pump pulse exactly transfers all population from the singlet to the triplet state (i.e. and exact optical π-pulse for this transition). In practice this will often not be the case, but for the essential aspects in our analysis this does not compromise its validity. Instead, an ultrafast pump pulse will in general bring the system in a quantum superposition of $|\psi_g\rangle$ and $|\psi_e(t = 0)\rangle$. However, the quantum coherence between these two states will typically decohere very fast, and this will bring the system in an incoherent mixture of $|\psi_g\rangle$ and $|\psi_e(t \approx 0)\rangle$. Then, the population in $|\psi_g\rangle$ will not contribute to the TRFR signal (for our probing scheme, see below). At the same time, the population in $|\psi_e(t \approx 0)\rangle$ will contribute to the TRFR signal in the same manner as a system that is purely in this state. The main reason to still aim for excitation with an optical π-pulse is that this maximizes the TRFR signal, and our estimates below here assume this case.

We thus assume that the pump pulse brings the molecules in a state that is purely a superposition of triplet sublevels ($|\psi_e(t)\rangle$ in Fig. 3.2b). This state will show coherent spin dynamics as a function of time (also at zero magnetic field the triplet sublevels are typically not degenerate[50]). We will study this by calculating both $\langle \mathbf{S} \rangle (t)$ and $\langle \mathbf{J} \rangle (t)$, where $\mathbf{J} = \mathbf{L} + \mathbf{S}$ is the total electronic angular momentum in conventional notation, and t is the time after the arrival of the pump pulse (to be clear, we use t for time in the system's free evolution, and Δt for the pump-probe delay). As commonly done in literature on spintronics[51], we will use the word spin for well-defined states of $\mathbf{J}$. The discussion will clarify whether a net spin orientation refers to a nonzero expectation value for $\mathbf{J}$ or $\mathbf{S}$.

For our calculations we focus on a molecule that contains a heavy-metal atom in order to have large SOC. In literature, usually density-functional theory (DFT) calculations are used to study such complexes theoretically, like e.g. for platinum porphyrins[45] and iridium complexes[52]. We use the more accurate combined CASSCF/CASPT2/RASSI–SO method instead, as introduced by Roos and Malmqvist[17, 18] in MOLCAS[23], in order to have a better basis for extracting physically relevant wave functions and spin expectation values. Since this is computationally a very expensive method, we chose the relatively small metal-organic complex (2,6-bis(aminomethyl)phenyl)(hydrido)platinum (to which we refer in this work as $PtN_2C_8H_{12}$ (Fig. 3.1)). Note that this molecule is (possibly) not chemically stable, in contrast to the related molecule[53] with Cl substituted for the H bound to Pt and $N(CH_3)_2$ for NH_2. However, it is computationally much less demanding and therefore more suitable for our proof of principle calculation.

The sublevels of the lowest triplet (including SOC) of $PtN_2C_8H_{12}$ are labeled as $|\psi_1\rangle$, $|\psi_2\rangle$ and $|\psi_3\rangle$ (Fig. 3.2 and Supplementary Information Fig. 3.9 (p. 84)). The energies of these levels with respect to $|\psi_g\rangle$ are 3.544, 3.558 and 3.564 eV respectively, as obtained from the CASPT2 calculation. The corresponding nonzero components of the transition dipole moments are $\langle \psi_1 | \, y \, |\psi_g\rangle \approx 0.0003 - i0.0112$ and $\langle \psi_3 | \, z \, |\psi_g\rangle \approx 0.0063$ in atomic units (where the conversion factor to SI-units is $8.47836 \cdot 10^{-30}$ Cm). In other words, a transition from $|\psi_g\rangle$ is allowed only with y and z polarized light to state $|\psi_1\rangle$ and $|\psi_3\rangle$, respectively, but forbidden to state $|\psi_2\rangle$. Having this type of selection rules for singlet-triplet transitions is a generic property of systems with C_{2v} symmetry (for details see Supplementary Information Sec. 3.12 (p. 83)), and introduces a way to selectively excite to (a specific superposition of) triplet sublevels. Such an imbalance in populating the triplet sublevels is essential for inducing spin orientation (see also below).

A spectrally broad pump pulse with polarization in both the y and z-direction can thus bring the system into a superposition of $|\psi_1\rangle$ and $|\psi_3\rangle$. From the CASPT2 calculations, an energy splitting $E_3 - E_1 = 20$ meV (30 THz angular frequency) has been obtained (Supplementary Information Table 3.3 (p. 83)). To simultaneously address $|\psi_1\rangle$ and $|\psi_3\rangle$, we thus need to use ultrashort laser pulses with an uncertainty in the photon energy given by $\sigma_{E_{ph}} > E_3 - E_1$. This requires that the time duration of the pulses does not exceed 16 fs (defined as the standard deviation of the envelope), as follows from the time−energy uncertainty relation.

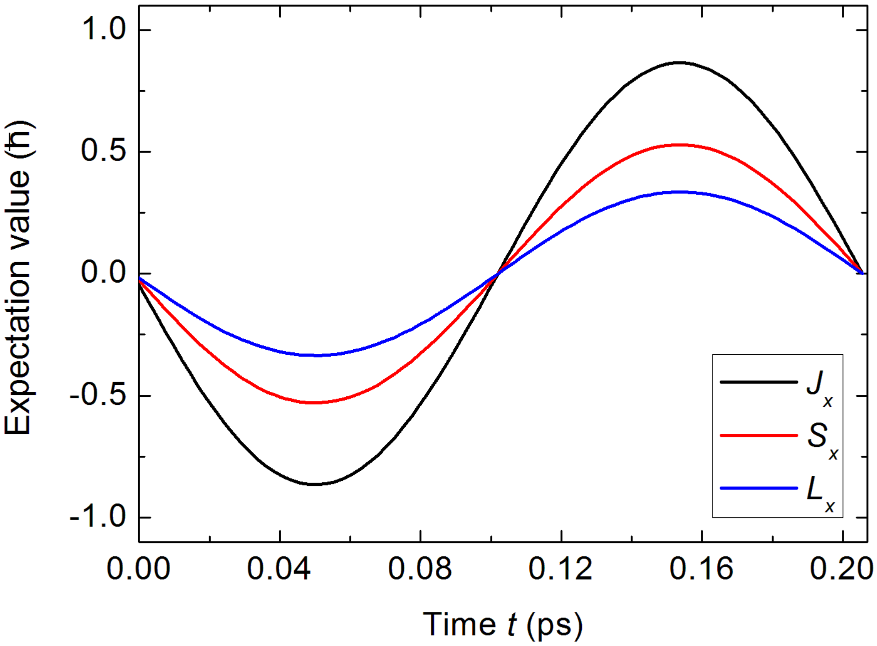

Figure 3.3: Calculation of $\langle J_x \rangle(t)$, $\langle L_x \rangle(t)$ and $\langle S_x \rangle(t)$ for a superposition of two triplet sublevels of a single $PtN_2C_8H_{12}$ molecule. This calculation originates from a superposition of triplet sublevels $|\psi_1\rangle$ and $|\psi_3\rangle$ (which interact with y and z polarized light respectively, Fig. 3.2), induced by an ultrashort pump pulse having electric unit vector $\hat{\mathbf{E}}_{pump} = \frac{\hat{\mathbf{z}}+\hat{\mathbf{y}}}{\sqrt{2}}$. Spin oscillation occurs in the x direction only. More specific, $\langle J_x \rangle(t)$, $\langle L_x \rangle(t)$ and $\langle S_x \rangle(t)$ oscillate with frequency $\omega_{31} = (E_3 - E_1)/\hbar$, while the y and z components remain zero.

For the pure triplet spin states T_x, T_y and T_z (defined in Supplementary Information Eq. (3.77-3.79) (p. 84)), all (x, y, z) components of $\langle \mathbf{S} \rangle$ are zero. Instead, for a superposition of these sublevels the net spin can be nonzero. More specifically, for a superposition of two of these spin states (say, T_i and T_j), the spin expectation value oscillates with only a nonzero component in the direction perpendicular to i and j, and with a frequency corresponding to the energy difference between the sublevels. To induce nonzero spin and subsequent spin dynamics for $PtN_2C_8H_{12}$, we therefore propose a direct excitation from $|\psi_g\rangle$ to the state $|\psi_e(t = 0)\rangle$, being a superposition of $|\psi_1\rangle$ and $|\psi_3\rangle$ (Fig. 3.2a, for details see Supplementary Information Eq. (3.26) (p. 67)). As a function of time, this superposition evolves as $|\psi_e(t)\rangle$ (Fig. 3.2b and Supplementary Information Eq. (3.28) (p. 67)), for which $\langle J_x \rangle (t)$, $\langle L_x \rangle (t)$ and $\langle S_x \rangle (t)$ oscillate with frequency $\omega_{31} = (E_3 - E_1)/\hbar$, while the y and z components remain zero. Fig. 3.3 shows the result of a calculation of such an oscillation, for the case where the electric unit vector of the pump pulse is $\hat{\mathbf{E}}_{pump} = \frac{\hat{\mathbf{z}}+\hat{\mathbf{y}}}{\sqrt{2}}$.

We aim to probe this oscillating spin (orientation) via Faraday rotation, which can be realized my measuring the polarization rotation $\Delta\theta$ (as introduced in Fig. 3.1). The optical transitions and selection rules that we have introduced in the above can be used for calculating $\Delta\theta$ (for details see Supplementary Information Sec. 3.7 (p. 64) and Sec. 3.8 (p. 66)). Fig. 3.4 shows results of such a calculation, for an ensemble of isolated and identically oriented $PtN_2C_8H_{12}$ molecules (e.g. realized by using a crystal host). We have assumed a detuned linearly polarized probe pulse, and present $\Delta\theta$ as a function of the delay time Δt between an ultrashort polarized pump and probe pulse. Taking a detuned probe (Fig. 3.2) limits probe-pulse induced population transfer back to the ground state, which allows to consider dispersion only[54]. We take a detuning where dispersion is near maximal, while probe absorption is strongly suppressed.

While we do not present the full equations for the above calculation in the main text (but in the Supplementary Information), we will discuss here some notable aspects. The polarization of the probe pulse after transmission $\mathbf{E}_{out}$ is affected when its components experience a different real part of the refractive index[16] (birefringence). A generic description of light-matter interaction in such a medium requires formulating the linear susceptibility and relative permittivity as a tensor. However, the refractive index does not have a tensor representation due to its square-root relation with these parameters[55]. Speaking about refractive indices only makes sense when a transformation is performed to the basis of the principal axes, which are the eigenvectors of the linear susceptibility tensor

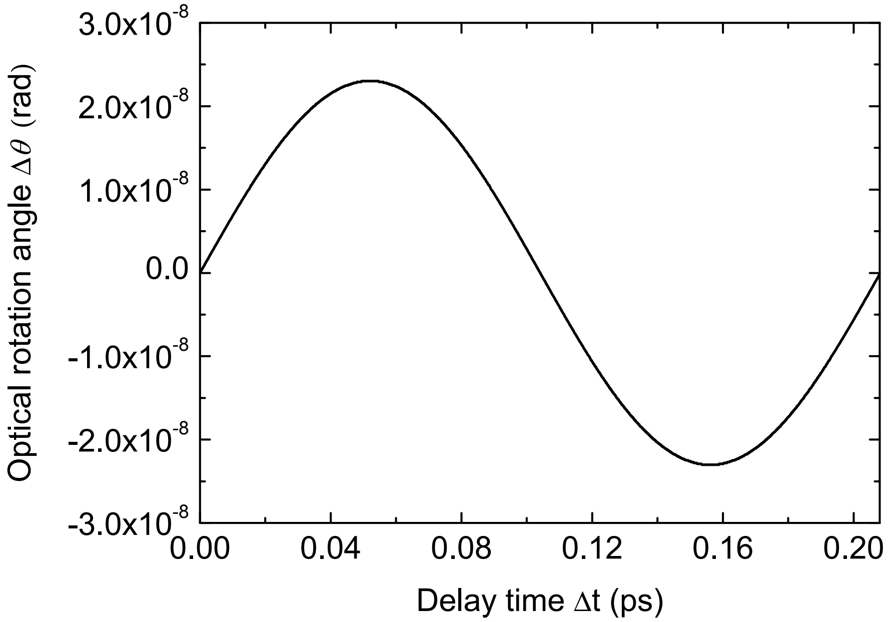

Figure 3.4: Calculation of the polarization rotation $\Delta\theta = \theta_{out} - \theta_{in}$ as a function of Δt for an ensemble of isolated and identically oriented $PtN_2C_8H_{12}$ molecules. The curve was calculated with Supplementary Information Eq. (3.61) (p. 73) with the following parameter values: Polarization parameters $\alpha = \beta = \delta = \varepsilon = 1/\sqrt{2}$, i.e. electric unit vectors $\hat{\mathbf{E}}_{pump} = \hat{\mathbf{E}}_{in} = \frac{\hat{\mathbf{z}}+\hat{\mathbf{y}}}{\sqrt{2}}$ (where $\hat{\mathbf{E}}_{in}$ is the initial polarization of the probe); Transition dipole moments $d_1 = 0.0003 - i0.0112$ and $d_3 = 0.0063$ a.u.; Triplet sublevel splitting $E_3 - E_1 = 20$ meV; Probe wavelength $\lambda = 349$ nm; Detuning $\Delta_p = -60$ meV, which is assumed to satisfy the requirements $|\Delta_p| >> \gamma$ and $|\Delta_p| >> |E_3 - E_1|/\hbar$; Thickness $d = 100$ nm; Number density $N = 10^{24}$ m^{-3}.

$\tilde{\boldsymbol{\chi}}^{(1)}$ (Eq. (3.31) in the Supplementary Information (p. 68)). For our system, the oscillating dynamics of $|\psi_e(t)\rangle$ yields that the principal axes oscillate with time (see Eq. (3.38) and (3.41)). While accounting for this, the electric-field components of the probe after transmission (Eq. (3.56)), and in turn the corresponding azimuth θ_{out} (Eq. (3.59)), and polarization rotation $\Delta\theta = \theta_{out} - \theta_{in}$ (Eq. (3.61)) can be calculated, for results as in Fig. 3.4.

Comparing Fig. 3.3 with Fig. 3.4, we conclude that $\Delta\theta(\Delta t)$ is an appropriate measure for $\langle \mathbf{J} \rangle (t)$, since both oscillate in phase with frequency ω_{31}. The experimental advantage of measuring oscillating coherent spin dynamics instead of merely spin orientation is that it is much easier to trace back the origin of a small signal when it oscillates, and it gives access to observing the dephasing time of the dynamics.

3.3 Feasibility analysis

The experimental feasibility of a molecular TRFR experiment particularly depends on the amplitude of the oscillation of the polarization rotation $\Delta\theta$ as a function of the delay time Δt. Typically, the accuracy of a TRFR experiment is in the order of nrads[56]. Fig. 3.4 gives a value of 23 nrad for this amplitude, well within the required range. In Supplementary Information Sec. 3.10 (p. 75) we discuss how this signal can be enhanced by several orders of magnitude. In the remainder of this section we address other aspects of the feasibility of a molecular TRFR experiment.

3.3.1 TRFR experiment with an ensemble of randomly oriented molecules

In Supplementary Information Sec. 3.15 (p. 91) we show for an ensemble of randomly oriented $PtN_2C_8H_{12}$ molecules that the TRFR signal is only reduced by a factor 2 as compared to the case with all molecules oriented such that the maximum signal is obtained (i.e. perpendicular to the incoming light). Hence, optically induced spin orientation does not necessarily require the same orientation for the molecules of interest when put in a crystal host. Moreover, this shows that a nonzero TRFR signal can be obtained for molecules in the gas phase and in solution. In these cases it can be satisfied that the molecules of interest are well isolated from each other. Still, the spin lifetime might be affected by several effects.

The spin dynamics might be affected by thermal fluctuations within the molecule. Although this is usually hardly the case for pure spins, the effect might be nonnegligible in our case due to the orbital part being mixed in via SOC. As long as this orbital contribution is small, these effects will not be severe. The strength of the SOC effect drives in fact a trade off between positive and negative effects for observing long-coherent spin oscillations with TRFR. Strong SOC makes the direct singlet-triplet transition stronger. However, it will also shorten the effective triplet-spin dephasing time because it shortens the optical life time of the triplet state, and since it enhances the mentioned coupling to thermal fluctuations. In addition, rapid tumbling of molecules in solution might limit for how long coherent spin oscillations can be observed. This effect might be suppressed by e.g. taking a high viscosity of the solvent, large molecules or a low temperature (for details see Supplementary Information Sec. 3.15). Another trade off lies in the triplet sublevel splitting for the system of choice. A larger splitting gives faster spin oscillations, but is thus more demanding on the need for ultrashort laser pulses. A larger energy scale for the splitting probably increases to what extent the spin dynamics couples to other dynamics of the system.

3.3.2 Single molecule TRFR experiment

In earlier work, the optically detected magnetic resonance (ODMR) technique has been used to study triplet spin polarization in molecular ensembles[57] and single molecules[58]. Within this technique, a microwave field drives the spin dynamics. An advantage of our TRFR technique may lie in that it is an all-optical technique, and fast laser pulses give access to a much higher time resolution. Other advantages are the absence of a magnetic field and the applicability to ensembles of randomly oriented molecules.

It would be very interesting to be able to also apply the TRFR experiment to a single molecule. Hence, we qualitatively determine whether such an experiment is possible. As an approximation for the signal obtained with a single molecule experiment, we can take the thickness d equal to the separation between two molecules (determined by N). In our calculation for $PtN_2C_8H_{12}$, we have $d =$ 100 nm and N corresponding to a separation of 10 nm. Our approximation thus implies only one order of magnitude loss of $\Delta\theta$ signal when taking a single molecule into account. We thus conclude that the signal of a TRFR experiment applied to a single $PtN_2C_8H_{12}$ molecule lies within the measurable range ($>$ nrad) which offers a strong indication that the TRFR technique can be used to probe the spin of single molecules as well. Likewise, the TRFR technique has already been applied successfully to probing of a single spin in a semiconductor quantum dot[59].

3.3.3 Franck-Condon suppression of optical transitions

Although our proof-of-principle calculation was performed for (2,6-bis(aminomethyl)phenyl)(hydrido)platinum, this particular molecule seems unfavorable for an actual demonstration of a molecular TRFR experiment since the Franck-Condon (FC) factor for the zero-phonon transition is extremely small (Supplementary Information Sec. 3.13 (p. 85)). Using the zero-phonon transition is still preferred to avoid a strongly disturbing coupling between the coherent spin dynamics and phonons. The zero-phonon-line FC factors for platinum porphyrins are much larger (Supplementary Information Sec. 3.13), which make them promising candidates for spintronics applications in general[45], and for a molecular TRFR experiment in particular (Supplementary Information Sec. 3.14 (p. 86)).

3.3.4 Persistence of spin-orientation effects for symmetries lower than C_{2v}

For our proof-of-principle study we have focused on a system with C_{2v} symmetry, for which the complexity of the description can be kept at a moderate level. This case is also relevant since many organic molecules have a flat structure (around the location with the optically active electrons). For molecules that only weakly deviate from this C_{2v} symmetry, the effects are most likely only weakly suppressed. That is, the effects demonstrated in this chapter only fade out gradually when one gradually distorts the C_{2v} symmetry.

The nonzero TRFR signal in our proposal comes mainly forward due to the strong selection rules that link particular optical polarizations to transitions from the singlet ground state into specific triplet sublevels. More specific, since one of the three electric dipole moments for the singlet-to-triplet transitions is zero (directly following from the C_{2v} symmetry), the TRFR signal shows a single spin oscillation, originating from the quantum superposition of two triplet sublevels. In the case of a relatively large deviation from C_{2v}, these selection rules become usually less strict in two ways: excitations are allowed (1) to all three sublevels, and (2) with all polarizations (x, y, z). However, the oscillator strengths of the different polarizations are usually not equally strong for the different sublevels. As such, an imbalance in the populations of the triplet sublevels can still be created, such that the TRFR signal will not be fully suppressed. Additionally, the total TRFR signal will then consist of a sum of three oscillations with frequencies $|\omega_{ij}| = |E_i - E_j|/\hbar$, with i and j two different triplet sublevel indices.

3.4 Summary and Outlook

We have derived the fundamentals of a TRFR experiment applied to organic molecules with strong spin-orbit coupling allowing for singlet-triplet excitations. We have shown how the optical selection rules can be exploited to induce a quantum superposition of triplet sublevels of the excited state of the molecular system, using an ultrashort pump pulse. We have derived how the polarization of an optical probe pulse is affected upon transmission, from which the requirements for polarization rotation follow. As a proof-of-principle calculation, the metal-organic complex (2,6-bis(aminomethyl)phenyl)(hydrido)platinum has been considered to study the possibility of a molecular TRFR experiment. Using the results of ab initio calculations, we have calculated the time dependence of the polarization rotation angle and of the expectation value of the total electronic angular momentum. Both oscillate in phase with a frequency corresponding to the sublevel splitting, implying that the oscillation of polarization rotation is a suitable measure for coherent spin dynamics. Nevertheless, metal-organic molecules like platinum porphyrins seem better candidates for a molecular TRFR experiment because of their larger Franck-Condon factors for the zero-phonon transition.

Using the TRFR technique to study triplet-exciton spin dynamics in organic molecules offers an interesting tool for probing material properties and new functionalities. An obvious example is a study of the lifetime of coherent spin dynamics, and the TRFR technique also allows for studying (extremely small or zero) energy splittings between triplet sublevels. Such studies are useful for judging whether the molecules can be applied in spintronic or quantum information applications via light-induced spin orientation, or sensors based on spin dynamics.

3.5 Author contributions

This chapter is based on Ref. 2 on p. 177. The project was initiated by C.H.W., R.W.A.H. and G.J.J.L. Derivations, calculations and data analysis were performed by G.J.J.L. and X.G. G.J.J.L. had the lead on writing the manuscript. All authors contributed to improving the manuscript. We acknowledge M. Wobben for her contribution to the calculation of Franck-Condon factors in several metal-organic molecules.

Supplementary Information (SI)

3.6 SI: Principles of the TRFR technique for an idealized $\Pi-$system

We give here the theoretical basis of the Time-Resolved Faraday Rotation (TRFR) technique (main text Fig. 3.1) as applied to the artificial system of Fig. 3.5 which contains a single electron and where a weak magnetic field is applied in the z-direction. For the sake of simplicity, we assume that the levels $|3\rangle$ and $|4\rangle$ lie significantly lower than the levels $|1\rangle$ and $|2\rangle$. As such, this system closely resembles quantum wells with a zinc-blende band structure having a conduction band that is derived from s-like atomic states and a valence band from p-like states. For such quantum wells, the concept of spin injection is discussed by Fox[10] (2nd ed., chapter 6.4.5).

The TRFR technique is a pump-probe technique, where a resonant pump pulse induces spin polarization and where the polarization rotation of a detuned (usually linearly polarized) probe pulse is measured as a function of delay time, as a measure for the spin dynamics of the system. We will assume that the photon energy of both the pump and probe pulses equals $E_{ph} = E_+ - E_2 = E_- - E_1$. As such, we can neglect $|3\rangle$ and $|4\rangle$, implying that the system behaves as a four-level Π-system. The physics behind the TRFR technique as applied to a Π-system (Fig. 3.5) offers a useful basis for this technique applied to V-systems like the singlet-triplet system on which the rest of this work focuses. Note that if the energies E_3 and E_4 would be equal to E_1 and E_2, the system would resemble direct gap III-V semiconductors (Fox[10], 2nd ed., chapter 3.3.7). As such, the concept of spin injection becomes slightly more complicated. Now, σ^+ and σ^- also allow for the transitions $|3\rangle_x \rightarrow |+\rangle_x$ and $|4\rangle_x \rightarrow |-\rangle_x$ respectively, though with a probability three times as small as the transitions depicted in Fig. 3.5. For direct gap III-V semiconductors, one can therefore induce at most 50% spin polarization.

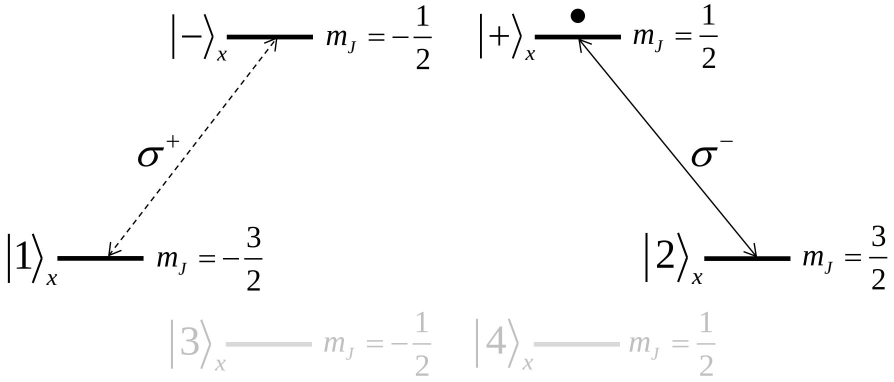
$|-\rangle_x$ $m_J=-\frac{1}{2}$
$|+\rangle_x$ $m_J=\frac{1}{2}$
σ^+
σ^-
$|1\rangle_x$ $m_J=-\frac{3}{2}$
$|2\rangle_x$ $m_J=\frac{3}{2}$
$|3\rangle_x$ $m_J=-\frac{1}{2}$
$|4\rangle_x$ $m_J=\frac{1}{2}$

Figure 3.5: Selection rules for circularly polarized light for an isolated system closely resembling a quantum well with the zinc-blende band structure. Using ultrashort pulses (with a Heisenberg uncertainty in E_{ph} larger than the Zeeman splittings), the optical selection rules apply to the quantization axis defined by the x-direction in which the pulses propagate (whereas the magnetic field is in the z-direction). For the sake of simplicity, we assume that the probe light is close to resonance with the transition to the states $|1\rangle$ and $|2\rangle$ such that we can neglect $|3\rangle$ and $|4\rangle$, implying that the system behaves as a four-level Π-system. Hence, the only nonzero transition dipole moments are $\mu_{-1}^{\sigma^+} = -e\ {}_x\langle -|\sigma^+|1\rangle_x \equiv -ed_1$ and $\mu_{+2}^{\sigma^-} = -e\ {}_x\langle +|\sigma^-|2\rangle_x \equiv -ed_2$. Spin polarization in the excited state is induced with a circularly polarized pump pulse ($\sigma^- = \frac{\hat{\mathbf{y}}-i\hat{\mathbf{z}}}{\sqrt{2}}$) which prepares the system in the state $|+\rangle_x$ (see Eq. (3.1)), where we assume full absorption for a system having initially only $|2\rangle_x$ populated. Directly after excitation, the wave function is given by $|+\rangle_x$. A magnetic field in the z-direction induces population transfer to $|-\rangle_x$. Accordingly, the wave function is given by Eq. (3.6) as a function of time. The polarization rotation of a linearly polarized probe pulse (originating from a different refractive index for its circular components) as a function of the delay time Δt is a suitable measure for the spin dynamics.

Let us consider (for the system in Fig. 3.5) a circularly polarized pump pulse propagating in the x-direction (corresponding to the so-called Voigt geometry, i.e. perpendicular to the magnetic field) with polarization $\sigma^- = \frac{\hat{\mathbf{y}}-i\hat{\mathbf{z}}}{\sqrt{2}}$. Using ultrashort laser pulses (with a Heisenberg uncertainty in E_{ph} larger than the Zeeman splittings), the optical selection rules apply to the quantization axis defined by the propagation direction. For light propagating in the x-direction, the relevant transition dipole moments for the system of Fig. 3.5 are $\mu_{-1}^{\sigma^+} = -e\ {}_x\langle -|\sigma^+|1\rangle_x \equiv -ed_1$ and $\mu_{+2}^{\sigma^-} = -e\ {}_x\langle +|\sigma^-|2\rangle_x \equiv -ed_2$. Note that $\mu_{-1}^{\sigma^-}$, $\mu_{+2}^{\sigma^+}$, μ_{-2} and μ_{+1} are zero according to the selection rules. Let us assume that the electron initially populates $|2\rangle_x$. Assuming full absorption, the pulse spin polarizes the system such that only the state $|+\rangle_x$ is populated, We use a subscript x to refer to the optical $\{|+\rangle_x, |-\rangle_x\}$-basis, and z to refer to the $\{|+\rangle_z, |-\rangle_z\}$-basis. Let us define for the wave function at time $t = 0$

$$|\psi_e(t=0)\rangle = |+\rangle_x = \frac{|+\rangle_z + |-\rangle_z}{\sqrt{2}} \tag{3.1}$$

The corresponding spin polarization amounts $\Pi = 1$, according to

$$\Pi = \left| \frac{N(+) - N(-)}{N(+) + N(-)} \right| \tag{3.2}$$

Due to the magnetic field, the spin undergoes a Larmor precession, since $|+\rangle_x$ is not an eigenstate of the Hamiltonian. As a function of time, the wave function is given by (neglecting decay processes)

$$|\psi_e(t)\rangle = \frac{\mathrm{e}^{-iE_+t/\hbar}|+\rangle_z + \mathrm{e}^{-iE_-t/\hbar}|-\rangle_z}{\sqrt{2}} \tag{3.3}$$

After multiplication with a global phase factor, and defining $\Omega = \frac{E_+ - E_-}{\hbar}$, this yields

$$|\psi_e(t)\rangle = \frac{|+\rangle_z + \mathrm{e}^{i\Omega t}|-\rangle_z}{\sqrt{2}} \tag{3.4}$$

For a TRFR experiment, the polarization rotation $\Delta\theta$ of a linearly polarized pump pulse is recognized to be a measure for the amount of spin polarization. Spin dynamics is studied experimentally by measuring $\Delta\theta$ as a function of the delay time Δt between the pump and probe. Let us derive $\Delta\theta(\Delta t)$ for a probe pulse propagating in the x-direction with $\mathbf{E}_{in} = E_0\hat{\mathbf{y}}$. The origin of a polarization rotation lies in a different (real part of the) refractive index for the circularly polarized components of the probe pulse. Written as a superposition of circular components, we have $\hat{\mathbf{y}} = \frac{\sigma^+ + \sigma^-}{\sqrt{2}}$. Note that the probe pulse is detuned in order to prevent population transfer. Since the selection rules for electronic dipole transitions apply in the optical basis, let us perform the transformation $|\psi_e(t)\rangle_z \rightarrow |\psi_e(t)\rangle_x$ using the transformation matrix

$$U_{S_z \rightarrow S_x} = \begin{bmatrix} \frac{1}{\sqrt{2}} & \frac{1}{\sqrt{2}} \\ \frac{1}{\sqrt{2}} & -\frac{1}{\sqrt{2}} \end{bmatrix} \tag{3.5}$$

This yields

$$|\psi_e(t)\rangle = \frac{1 + \mathrm{e}^{i\Omega t}}{2}|+\rangle_x + \frac{1 - \mathrm{e}^{i\Omega t}}{2}|-\rangle_x \tag{3.6}$$

To determine the refractive indices, let us first consider the linear susceptibility tensor $\tilde{\boldsymbol{\chi}}^{(1)}$, with components given by Boyd[54] (3rd Ed. Eq. (3.5.18))

$$\tilde{\chi}^{(1)}_{ij}(\omega_p) = \frac{N}{\varepsilon_0\hbar}\sum_{nm}\rho^{(0)}_{mm}\left[\frac{\mu^i_{mn}\mu^j_{nm}}{(\omega_{nm}-\omega_p)-i\gamma_{nm}}+\frac{\mu^i_{nm}\mu^j_{mn}}{(\omega_{nm}+\omega_p)+i\gamma_{mn}}\right] \tag{3.7}$$

where we use a tilde to denote a complex number. Here, we consider an ensemble with N the number density of isolated systems (each represented by Fig. 3.5), $\varepsilon_0 = 8.854...\cdot 10^{-12}\ \mathrm{F\,m^{-1}}$ is the vacuum permittivity, $\hbar = 1.054...\cdot 10^{-34}\ \mathrm{J\,s}$ is Planck's constant, $\rho^{(0)}_{mm}$ is the first term in a power series for the diagonal elements of the density matrix, $\mu^i_{en} = -e\langle\psi_e(t)|i|\psi_n\rangle$ is the i-component of the transition dipole moment (with $i = x, y, z$), $\omega_{mn} = (E_m - E_n)/\hbar$ is the transition frequency, ω_p is the probe laser frequency, and γ is the damping rate. Note that in Eq. (3.7) ε_0 should be omitted when using Gaussian units (as in older editions of Boyd) instead of SI-units.

When the probe pulse arrives at the sample, the system (Fig. 3.5) populates the excited state given by Eq. (3.6). This implies that $\rho^{(0)}_{ee} = 1$, whereas $\rho^{(0)}_{11} = \rho^{(0)}_{22} = 0$. Since the levels $|1\rangle_x$ and $|2\rangle_x$ are empty, only the (detuned) downward transitions $|-\rangle_x \to |1\rangle_x$ and $|+\rangle_x \to |2\rangle_x$ are relevant for the description of the polarization rotation (since an upward transition with the probe is impossible with zero population in the lower states). This implies that the second term in Eq. (3.7) corresponds to resonance and is the so-called rotating term, whereas the first term is the counter-rotating one and can be omitted. Hence, we can write the components of the linear susceptibility tensor $\tilde{\boldsymbol{\chi}}^{(1)}$ to a good approximation as

$$\tilde{\chi}^{(1)}_{ij}(\omega_p) = \frac{N}{\varepsilon_0\hbar}\sum_{n=1}^{2}\frac{\mu^i_{ne}\mu^j_{en}}{\Delta_{p,ne}+i\gamma_{ne}} \tag{3.8}$$

where we define $\Delta_{p,ne} = \omega_{ne} + \omega_p$. The eigenvectors of $\tilde{\boldsymbol{\chi}}^{(1)}$ are the so-called principal axes. For a probe pulse propagating in the x-direction, we can neglect the x-components of $\tilde{\boldsymbol{\chi}}^{(1)}$. The other two principal axes turn out to be $\sigma^+ = \frac{\hat{\mathbf{y}}+i\hat{\mathbf{z}}}{\sqrt{2}}$ and $\sigma^- = \frac{\hat{\mathbf{y}}-i\hat{\mathbf{z}}}{\sqrt{2}}$, with corresponding transition dipole moments

$$\mu^{\sigma^+}_{e1} = -e\ {}_x\langle\psi_e(\Delta t)|\sigma^+|1\rangle_x = -e\frac{1-\mathrm{e}^{-i\Omega\Delta t}}{2}d_1 = \left(\mu^{\sigma^+}_{1e}\right)^* \tag{3.9}$$

$$\mu^{\sigma^-}_{e2} = -e\ {}_x\langle\psi_e(\Delta t)|\sigma^-|2\rangle_x = -e\frac{1+\mathrm{e}^{-i\Omega\Delta t}}{2}d_2 = \left(\mu^{\sigma^-}_{2e}\right)^* \tag{3.10}$$

In the $\{\sigma^+, \sigma^-\}$-basis the only nonzero components of $\tilde{\boldsymbol{\chi}}^{(1)}$ are

$$\tilde{\chi}^{(1)}_{\sigma^+\sigma^+} = \frac{N}{\varepsilon_0\hbar}\frac{\mu^{\sigma^+}_{1e}\mu^{\sigma^+}_{e1}}{\Delta_{p,1e}+i\gamma_{1e}} = \frac{N}{\varepsilon_0\hbar}\frac{e^2|d_1|^2}{\Delta_{p,1e}+i\gamma_{1e}}\frac{1-\cos(\Omega\Delta t)}{2} \tag{3.11}$$

$$\tilde{\chi}^{(1)}_{\sigma^-\sigma^-} = \frac{N}{\varepsilon_0\hbar}\frac{\mu^{\sigma^-}_{2e}\mu^{\sigma^-}_{e2}}{\Delta_{p,2e}+i\gamma_{2e}} = \frac{N}{\varepsilon_0\hbar}\frac{e^2|d_2|^2}{\Delta_{p,2e}+i\gamma_{2e}}\frac{1+\cos(\Omega\Delta t)}{2} \tag{3.12}$$

Assuming $d_1 = d_2 \equiv d_0$, $\Delta_{p,1e} = \Delta_{p,2e} \equiv \Delta_p$ and $\gamma_{1e} = \gamma_{2e} \equiv \gamma$ allows us to write

$$\tilde{\boldsymbol{\chi}}^{(1)} = \frac{Ne^2|d_0|^2}{\varepsilon_0\hbar}\frac{\Delta_p - i\gamma}{\Delta_p^2+\gamma^2}\begin{bmatrix} \frac{1-\cos(\Omega\Delta t)}{2} & 0 \\ 0 & \frac{1+\cos(\Omega\Delta t)}{2}\end{bmatrix} \tag{3.13}$$

Clearly, $\tilde{\boldsymbol{\chi}}^{(1)}$ depends on Δt. However, since $\tilde{\boldsymbol{\chi}}^{(1)}$ is diagonal (independent of Δt), the principal axes do not depend on Δt. It is important to realize that we have considered a Π-system here. In Section 3.8 we will consider a V-system for which the principal axes turn out to oscillate as a function of Δt.

To determine how the circular components of a linear probe are affected upon transmission, we have to consider their refractive indices. The refractive index is given by[54]

$$\tilde{n}_j = \sqrt{1+\tilde{\chi}^{(1)}_{jj}} \approx 1 + \frac{1}{2}\tilde{\chi}^{(1)}_{jj} \tag{3.14}$$

where the latter approximation is valid for $\left|\tilde{\chi}^{(1)}_{jj}\right| << 1$. We assume that the probe is sufficiently detuned from the $|-\rangle \rightarrow |1\rangle$ and $|+\rangle \rightarrow |2\rangle$ transitions, such that the imaginary part of $\tilde{\boldsymbol{\chi}}^{(1)}$ can be neglected, and with that population transfer as well (as explained in Section 3.7). From Eq. (3.13) and Eq. (3.14) it follows that the difference between the real parts of the refractive indices amounts

$$\Delta n \equiv n_{\sigma^-} - n_{\sigma^+} \approx \frac{Ne^2|d_0|^2}{\varepsilon_0\hbar}\frac{\Delta_p}{\Delta_p^2+\gamma^2}\frac{\cos(\Omega\Delta t)}{2} \tag{3.15}$$

To describe how the probe pulse is affected by the sample, one should consider the Jones matrix $J\{\sigma^+,\sigma^-\}$, which performs the following transformation

$$\mathbf{E}_{out}\{\sigma^+,\sigma^-\} = J\{\sigma^+,\sigma^-\}\mathbf{E}_{in}\{\sigma^+,\sigma^-\} = J\{\sigma^+,\sigma^-\}\begin{bmatrix} E_0/\sqrt{2} \\ E_0/\sqrt{2}\end{bmatrix} \tag{3.16}$$

The Jones matrix is given by

$$J\{\sigma^+,\sigma^-\} = \begin{bmatrix} \mathrm{e}^{i\Lambda n_{\sigma^+}} & 0 \\ 0 & \mathrm{e}^{i\Lambda n_{\sigma^-}}\end{bmatrix} \tag{3.17}$$

which expresses the retardation of (light polarized along) principal axis $\hat{\mathbf{j}}$ by Λn_j where $\Lambda \equiv 2\pi d/\lambda$, with d the thickness of the sample and λ the wavelength of the light[16]. It is more convenient to multiply the Jones vector with the global phase factor $\mathrm{e}^{-i\Lambda n_{\sigma^+}}$ which gives for Eq. (3.16)

$$\mathbf{E}_{out}\{\sigma^+,\sigma^-\} = \frac{E_0}{\sqrt{2}}\begin{bmatrix}1\\ \mathrm{e}^{i\Lambda\Delta n}\end{bmatrix} \tag{3.18}$$

To determine the polarization rotation we follow the circular complex-plane representation of polarized light as defined in the book of Azzam and Bashara[16]. In line with Eq. (1.92) of [16] we define the ratio

$$\kappa = E_{\sigma^+}/E_{\sigma^-} \tag{3.19}$$

where we use κ in contrast to [16] (which uses χ). From Eq. (1.95) of [16] we adopt the expression for the azimuth θ

$$\theta = -\frac{\arg(\kappa)}{2} \tag{3.20}$$

For the incoming and outcoming probe, Eq. (3.19) yields $\kappa_{in} = 1$ and $\kappa_{out} = \mathrm{e}^{-i\Lambda\Delta n}$, corresponding to $\theta_{in} = 0$ and $\theta_{out} = \frac{\Lambda\Delta n}{2}$ respectively, according to Eq. (3.20). The polarization rotation (optical rotation angle) $\Delta\theta$ is now given by

$$\Delta\theta = \theta_{out} - \theta_{in} \tag{3.21}$$

which gives $\Delta\theta = \frac{\pi d\Delta n}{\lambda}$, with Δn proportional to $\cos(\Omega\Delta t)$ as given by Eq. (3.15). Measuring $\Delta\theta$ as a function of Δt will show an oscillation with angular frequency $\Omega = \frac{E_+ - E_-}{\hbar}$ and amplitude

$$max(\Delta\theta) = \frac{\pi d}{2\lambda}\frac{Ne^2|d_0|^2}{\varepsilon_0\hbar}\frac{\Delta_p}{\Delta_p^2+\gamma^2} \tag{3.22}$$

In literature[13, 46] this oscillation of the polarization rotation is recognized to be a suitable measure for the Larmor spin precession in the excited state, since the angular frequency is the same for both oscillations. The reader is referred to the book of Cohen-Tannoudji, Diu and Laloë[5] for a derivation of the oscillation of a Larmor spin precession of a spin 1/2 in the presence of a uniform magnetic field: for a spin initially populating the state $|+\rangle_x$, the angular frequency of the time-variation of the expectation value $\langle S_x\rangle$ equals the energy splitting between the sublevels (in units of $\hbar$) induced by the field.

So far, we considered an ensemble of isolated Π-systems (with number density N), where each system is represented by Fig. 3.5. Let us now shortly elaborate on how to theoretically describe a TRFR experiment applied to a coherently coupled ensemble of Π-systems (with number density N). We will see that also the upward transitions affect the probe polarization and contribute to the total TRFR signal.

A pump pulse driving the upward transition $|2\rangle_x \to |+\rangle_x$ does not only induce electron spin polarization in the state $|+\rangle_x$. Simultaneously, the hole spin in the state $|2\rangle_x$ ($m_J = 3/2$) is polarized. However, e.g. in III-V direct gap semicondutors the corresponding hole spin dynamics in the valence band is usually neglected (i.e. an equal distribution of the valence band states is assumed) because of the fast thermalization (particularly because the valence bands with $m_J = -1/2, 1/2$ lie closeby), happening on a much shorter timescale than the conduction band's electron spin dynamics. Nevertheless, the probe polarization will be affected also by the (detuned) upward transitions $|1\rangle_x \to |-\rangle_x$ and $|2\rangle_x \to |+\rangle_x$, since the hole spin in the conduction band is polarized as well. Here, the reader is referred to Fig. 3.5, but one should now understand the bars as bands. Also, there is now (partial) population in the valence band states ($|1\rangle_x$ up to $|4\rangle_x$). Particularly interesting is the case where thermalization of the valence band states does not occur faster than the spin dynamics in the conduction band, as can e.g. be realized for quantum wells with a zinc-blende band structure where the valence band states $|3\rangle_x$ and $|4\rangle_x$ lie sufficiently low. Accordingly, Larmor spin precession happens also in the valence band, accompanied by population transfer between the bands with $m_J = -3/2$ and $3/2$. Correspondingly, one can write down a time-dependent ground state (analogous to Eq. (3.6)) and follow the procedure as above for calculation of the refractive indices and resulting polarization rotation for a linearly polarized probe pulse.

One might wonder whether the contributions from the downward and upward transitions do not cancel. To show that this is not the case, let us consider the case where the probe pulse arrives at the sample directly after spin polarization with the pump pulse, i.e. $\Delta t = 0$. Let us consider the contributions separately by considering first (Case I) an artificial system as in Fig. 3.5, with only $|+\rangle_x$ populated, i.e. $\rho_{++}^{(0)} = 1$, and secondly (Case II) an artificial system as in Fig. 3.5, with only $|1\rangle_x$ populated, i.e. $\rho_{11}^{(0)} = 1$.

Case I: $\rho_{++}^{(0)} = 1$. This case simply follows from the theory above, where we can substitute $\Delta t = 0$ in Eq. (3.6) and replace the subscript e by $+$ in Eq. (3.8). It follows that the only nonzero component of $\tilde{\boldsymbol{\chi}}^{(1)}$ is

$$\tilde{\chi}^{(1)}_{\sigma_-\sigma_-}(\omega_p) = \frac{N}{\varepsilon_0\hbar}\frac{\mu_{2+}^{\sigma_-}\mu_{+2}^{\sigma_-}}{(\omega_{2+}+\omega_p)+i\gamma_{2+}} = \frac{N}{\varepsilon_0\hbar}\frac{|\mu|^2}{\Delta_p + i\gamma} = \frac{N}{\varepsilon_0\hbar}|\mu|^2\frac{\Delta - i\gamma}{\Delta_p^2+\gamma^2} \quad (3.23)$$

where we have defined (in line with the theory above) $\Delta_p \equiv \omega_{2+} + \omega_p$ where

$\omega_{2+} = (E_2 - E_+)/\hbar < 0$. Also, we assume $\gamma_{2+} = \gamma_{-1} \equiv \gamma$ and $\mu^{\sigma_-}_{2+} = \mu^{\sigma_+}_{1-} \equiv \mu$.

Case II: $\rho^{(0)}_{11} = 1$. For this case the wave function is given by $|1\rangle_x$. For the linear susceptibility this implies that the first term in Eq. (3.6) corresponds to resonance and is the so-called rotating term, whereas the second term is the counter-rotating one and can be omitted. It follows that the only nonzero component of $\tilde{\boldsymbol{\chi}}^{(1)}$ is

$$\tilde{\chi}^{(1)}_{\sigma_+\sigma_+}(\omega_p) = \frac{N}{\varepsilon_0\hbar}\frac{\mu^{\sigma_+}_{1-}\mu^{\sigma_+}_{-1}}{(\omega_{-1}-\omega_p)-i\gamma_{-1}} = \frac{N}{\varepsilon_0\hbar}\frac{|\mu|^2}{-\Delta_p - i\gamma} = \frac{N}{\varepsilon_0\hbar}|\mu|^2\frac{-\Delta+i\gamma}{\Delta_p^2+\gamma^2} \qquad (3.24)$$

where $\omega_{-1} = (E_- - E_1)/\hbar > 0$. Also, we have $\omega_{-1} = -\omega_{2+}$, which implies $\omega_{-1} - \omega_p = -\Delta_p$.

We see that $\tilde{\chi}^{(1)}_{\sigma_+\sigma_+}(\omega_p)$ in Eq. (3.24) equals $-\tilde{\chi}^{(1)}_{\sigma_-\sigma_-}(\omega_p)$ in Eq. (3.23). For a coherent ensemble (e.g. a quantum well with a zinc-blende band structure) of the systems in Fig. 3.5 one might have that both the downward and upward transitions contribute to the total TRFR signal, thereby resembling Case I and Case II simultaneously. Considering the extreme (i.e. $\rho^{(0)}_{mm} = 1$) cases of Eq. (3.23) and Eq. (3.24), following Eq. (3.14) and Eq. (3.15) shows that at $\Delta t = 0$ the total TRFR amplitude can become twice the value of Eq. (3.22). In practice, one will not realize $\rho^{(0)}_{mm} = 0, 1$ (i.e. completely full or empty bands) for a coherent ensemble. The total TRFR signal will therefore be mitigated, but it is important to realize that both the downward and upward transitions can contribute to a polarization rotation of the probe pulse.

3.7 SI: Fundamentals of a molecular TRFR experiment

Let us study here the theoretical application of the Time-Resolved Faraday Rotation (TRFR) technique (main text Fig. 3.1) to a model system (main text Fig. 3.2) in the absence of a magnetic field. The system consists of the states $|\psi_g\rangle$, $|\psi_1\rangle$, $|\psi_2\rangle$ and $|\psi_3\rangle$, with energies E_g, E_1, E_2 and E_3, respectively, with $E_g = 0$. The only nonzero components of the transition dipole moments related to $|\psi_g\rangle$ are $\mu^y_{1g} = -e\langle\psi_1|y|\psi_g\rangle = -ed_1$ and $\mu^z_{3g} = -e\langle\psi_3|z|\psi_g\rangle = -ed_3$, with e the elementary charge. Considering absorption, the system behaves therefore as a three-level V-system where $|\psi_2\rangle$ can be neglected, but it is nevertheless displayed (main text Fig. 3.2) since in this work the excited state levels are sublevels of a triplet. In this regard it is interesting to mention the V-system of a GaAs quantum well, which has been studied theoretically[60] and for which electron spin dynamics experiments have been performed[61, 62]. In these experiments, a magnetic field ensures Larmor spin precession. Although we do not consider a magnetic field, most of the theory of Sections 3.7 and 3.8 can be directly applied to this V-system.

Although ultrashort pulses with a substantial energy uncertainty will be considered, monochromatic waves are assumed, for which (by definition) the time variation of the electric (field) vector $\mathbf{E}$ is exactly sinusoidal. Usually within the Jones formalism[63], the electric vector is denoted as $\mathbf{E} = E_x\hat{\mathbf{x}} + E_y\hat{\mathbf{y}}$, with $\hat{\mathbf{x}}$ and $\hat{\mathbf{y}}$ the orthonormal Jones unit vectors. In this work however, the propagation of light will be taken along the x-direction, such that the electric vector has nonzero components only in the y and z-direction.

At $t = 0$, an ultrashort pump pulse, for which the electric vector is given by $\mathbf{E}_{pump} = \alpha\hat{\mathbf{z}} + \beta\hat{\mathbf{y}}$ (with α and β in general complex), excites the system of main text Fig. 3.2a to $|\psi_e\rangle$, being a superposition of the states $|\psi_1\rangle$ and $|\psi_3\rangle$. The following assumptions are made: (*i*) Before the pump arrives, only $|\psi_g\rangle$ is populated, (*ii*) the photon energy is $E_{ph} = \frac{E_3+E_1}{2}$, with (*iii*) a quantum uncertainty $\sigma_{E_{ph}} > |E_3 - E_1|$, where a block function is assumed for the intensity distribution of the pulse instead of a Gaussian, and (*iv*) only $|\psi_e\rangle$ is populated after excitation with the pump pulse (i.e. full absorption).

Consider a sample, consisting of a homogeneous ensemble of these model systems with number density N. To ensure that the systems are well isolated from each other, N should be relatively small, which can be realized by putting the molecules in a molecular host crystal (i.e. a matrix) or liquid host (i.e. in solution), which should be transparent to the pump and probe pulse, or taking an ensemble of molecules in gas phase. In our derivation (Sec. 3.8 and 3.9) and calculations (Sec. 3.10) we will first assume that all molecules are oriented similarly, which can be realized via a (solid) host crystal. Later (Sec. 3.15), we will show that a net TRFR signal can even be obtained for an ensemble of randomly oriented molecules. Considering the host crystal, we assume that (*iv*) is satisfied for each system of the ensemble. In practice, it is sufficient when the vast majority of the systems satisfies (*iv*). Still, this will usually require the tuning of a very intense pump pulse, given the typical small transition dipole moment between ground and excited state. It is assumed that each system is evolving according to Eq. (3.27). After a delay time Δt, the sample is illuminated with an ultrashort probe pulse (also obeying assumptions (*ii*) and (*iii*)) for which the electric vector is given by $\mathbf{E}_{in} = \delta\hat{\mathbf{z}} + \varepsilon\hat{\mathbf{y}}$, to which we refer as the incoming probe.

Given the small transition dipole moment, the probability for a created exciton to recombine during the delay time between pump and probe is small as well.

Hence, it is reasonable to assume that the system has still no population in $|\psi_g\rangle$ once the probe pulse arrives at the sample (main text Fig. 3.2b). If one would now take a resonant probe pulse, all population would be transferred to $|\psi_g\rangle$ via stimulated emission, which is unfavourable in view of the lifetime of the spin dynamics. In this work therefore, we will assume that we are allowed to consider only the dispersion (related to stimulated emission). This implies neglecting $\left|\mathrm{Im}\left\{\tilde{\chi}^{(1)}_{ij}\right\}\right|$ with respect to $\left|\mathrm{Re}\left\{\tilde{\chi}^{(1)}_{ij}\right\}\right|$, with $\tilde{\boldsymbol{\chi}}^{(1)}$ the linear susceptibility tensor (see Eq. (3.29), as adapted from Boyd[54]). This can be realized by taking an off-resonant probe pulse (as illustrated in Fig. 3.2b) having a detuning $\Delta_p = \omega_{ge} + \omega_p$ (with $\omega_{ge} = (E_g - E_e)/\hbar < 0$ the transition frequency and $\omega_p > 0$ the probe laser frequency). Since $\tilde{\chi}^{(1)}_{ij}$ is proportional to $\frac{\Delta_p - i\gamma}{\Delta_p^2+\gamma^2}$, we can neglect $\left|\mathrm{Im}\left\{\tilde{\chi}^{(1)}_{ij}\right\}\right|$ if we ensure $|\Delta_p| >> \gamma$, which for the remaining real part implies $\frac{\Delta_p}{\Delta_p^2+\gamma^2} \approx \Delta_p^{-1}$. It is also instructive to plot the real and imaginary part of $\tilde{\chi}^{(1)}_{ij}$ as a function of ω_p (Boyd[54], 3rd ed., Fig. 3.5.1), illustrating that the tails of $\mathrm{Im}\left\{\tilde{\chi}^{(1)}_{ij}\right\}$ fall off faster than the ones of $\mathrm{Re}\left\{\tilde{\chi}^{(1)}_{ij}\right\}$. Note that we have defined the excited state $|\psi_e\rangle$ being a superposition of $|\psi_1\rangle$ and $|\psi_3\rangle$. However, it is somewhat misleading to consider for the calculation of Δ_p an energy E_e, since $|\psi_e\rangle$ is not an eigenstate of the Hamiltonian (naturally, one would take the expectation value $E_e = \langle\psi_e|H|\psi_e\rangle$). Strictly speaking, a probe laser has a different detuning with respect to the levels $|\psi_1\rangle$ and $|\psi_3\rangle$. However, we will use one and the same value for Δ_p for both $|\psi_1\rangle$ and $|\psi_3\rangle$ (within the calculation of $\tilde{\boldsymbol{\chi}}^{(1)}$ for a superposition of $|\psi_1\rangle$ and $|\psi_3\rangle$), which is a reasonable assumption if we take $|\Delta_p| >> |E_3 - E_1|/\hbar$.

To explain the requirements for the polarization rotation $\Delta\theta$ to oscillate as a function of the delay time Δt, both the general (Section 3.8) and an idealized (Section 3.9) scenario are considered.

3.8 SI: Polarization rotation for a TRFR experiment applied to a V-system

Here we derive the polarization of an ultrashort detuned probe pulse ($\mathbf{E}_{in} = \delta\hat{\mathbf{z}} + \varepsilon\hat{\mathbf{y}}$), as a function of the delay time Δt after the arrival of an ultrashort pump pulse ($\mathbf{E}_{pump} = \alpha\hat{\mathbf{z}} + \beta\hat{\mathbf{y}}$), for a model system as in main text Fig. 3.2 (nonzero μ^y_{1g} and μ^z_{3g}).

For the general case of full absorption of a pump pulse having $\mathbf{E}_{pump} = \xi\hat{\mathbf{x}} + \beta\hat{\mathbf{y}} + \alpha\hat{\mathbf{z}}$, for a system initially populated in $|\psi_i\rangle$, the state directly after a coherent excitation becomes

$$|\psi(t=0)\rangle = C\sum_n \langle\psi_n|\xi x + \beta y + \alpha z|\psi_i\rangle|\psi_n\rangle \tag{3.25}$$

with n the amount of involved excited state levels, and C the normalization factor. It is assumed that the pump pulse has an equal intensity for all energies $E_n - E_i$ (block pulse).

In our case, the superposition of states directly after excitation becomes

$$|\psi_e(t=0)\rangle = \frac{\beta d_1|\psi_1\rangle + \alpha d_3|\psi_3\rangle}{\sqrt{|\beta d_1|^2 + |\alpha d_3|^2}} \tag{3.26}$$

According to the time-dependent Schrödinger equation, this wave function evolves as

$$|\psi_e(t)\rangle = \frac{\mathrm{e}^{-iE_1 t/\hbar}\beta d_1|\psi_1\rangle + \mathrm{e}^{-iE_3 t/\hbar}\alpha d_3|\psi_3\rangle}{\sqrt{|\beta d_1|^2 + |\alpha d_3|^2}} \tag{3.27}$$

For convenience, Eq. (3.27) is multiplied with the global phase factor $\mathrm{e}^{iE_1 t/\hbar}$ to give

$$|\psi_e(t)\rangle = \frac{\beta d_1|\psi_1\rangle + \mathrm{e}^{i\Omega t}\alpha d_3|\psi_3\rangle}{\sqrt{|\beta d_1|^2 + |\alpha d_3|^2}} \tag{3.28}$$

with $\Omega \equiv \omega_{13} = (E_1 - E_3)/\hbar$.

The polarization of a probe pulse upon transmission, i.e. $\mathbf{E}_{out}$, might be affected, which follows from considering the linear susceptibility tensor $\tilde{\boldsymbol{\chi}}^{(1)}$. Assuming that for each system only $|\psi_e(t)\rangle$ is populated (Fig. 3.2b), following Boyd[54] (3rd ed., Eq. (3.5.20)) gives

$$\tilde{\chi}_{ij}^{(1)}(\omega_p) = \frac{N}{\varepsilon_0\hbar}\sum_n\left[\frac{\mu_{en}^i\mu_{ne}^j}{\Delta'_{p,ne} - i\gamma_{ne}} + \frac{\mu_{ne}^i\mu_{en}^j}{\Delta_{p,ne} + i\gamma_{ne}}\right] \tag{3.29}$$

where we use a tilde to denote a complex number. Here, N is the system's number density, $\varepsilon_0 = 8.854...\cdot 10^{-12}\ \mathrm{F\,m^{-1}}$ is the vacuum permittivity, $\hbar = 1.054...\cdot 10^{-34}$ $\mathrm{J\,s}$ is Planck's constant, $\mu_{en}^i = -e\langle\psi_e(t)|i|\psi_n\rangle$ with $i = x, y, z$, $\Delta'_{p,ne} = \omega_{ne} - \omega_p$ and $\Delta_{p,ne} = \omega_{ne} + \omega_p$ with ω_p the probe laser frequency, γ_{ne} is the damping rate. Note that in Eq. (3.29) ε_0 should be omitted when using Gaussian units (as in older editions of Boyd[54]) instead of SI-units.

Assuming that the laser can only address the ground state (via stimulated emission), we can drop the summation sign and substitute g for n, which yields

$$\tilde{\chi}_{ij}^{(1)}(\omega_p) = \frac{N}{\varepsilon_0\hbar}\left[\frac{\mu_{eg}^i\mu_{ge}^j}{\Delta'_p - i\gamma} + \frac{\mu_{ge}^i\mu_{eg}^j}{\Delta_p + i\gamma}\right] \tag{3.30}$$

where we have dropped the subscript n for Δ_p, Δ'_p and γ. Since the transition frequency $\omega_{ge} = (E_g - E_e)/\hbar < 0$ (and $\omega_p > 0$), only the second term in Eq. (3.30) can become resonant, and is therefore the rotating term (and the first the counter-rotating term). Within this rotating wave approximation the first term is therefore neglected when ω_p is nearly resonant with the transition frequency ω_{ge}. To a good approximation the linear susceptibility now becomes (after rewriting)

$$\tilde{\chi}^{(1)}_{ij}(\omega_p) = \frac{N}{\varepsilon_0 \hbar} \mu^i_{ge} \mu^j_{eg} \frac{\Delta_p - i\gamma}{\Delta_p^2 + \gamma^2} \tag{3.31}$$

where the detuning $\Delta_p = \omega_{ge} + \omega_p$ is positive for $\omega_p > |\omega_{ge}|$ and negative when $\omega_p < |\omega_{ge}|$.

The polarization of the probe pulse upon transmission $\mathbf{E}_{out}$ is affected when its components experience a different real part of the refractive index[16]. The refractive index does not have a tensor representation, due to the square root relationship with the dielectric constant[55]. Hence, speaking about refractive index only makes sense when a transformation is performed to the basis of the principal axes, which are the eigenvectors of $\tilde{\boldsymbol{\chi}}^{(1)}$. To determine these, we first write down the (only nonzero) transition dipole moments

$$\begin{aligned}\mu^z_{eg} = \left(\mu^z_{ge}\right)^* &= -e\langle\psi_e(\Delta t)|z|\psi_g\rangle \\ &= -e\left(\frac{\beta^* d_1^* \langle\psi_1| + \mathrm{e}^{-i\Omega\Delta t}\alpha^* d_3^*\langle\psi_3|}{\sqrt{|\beta d_1|^2 + |\alpha d_3|^2}}\right) z|\psi_g\rangle \\ &= -e\frac{\mathrm{e}^{-i\Omega\Delta t}\alpha^*|d_3|^2}{\sqrt{|\beta d_1|^2 + |\alpha d_3|^2}}\end{aligned} \tag{3.32}$$

$$\begin{aligned}\mu^y_{eg} = \left(\mu^y_{ge}\right)^* &= -e\langle\psi_e(\Delta t)|y|\psi_g\rangle \\ &= -e\frac{\beta^*|d_1|^2}{\sqrt{|\beta d_1|^2 + |\alpha d_3|^2}}\end{aligned} \tag{3.33}$$

Neglecting constant prefactors, diagonalization of $\tilde{\boldsymbol{\chi}}^{(1)}$ involves diagonalization of the matrix

$$\begin{bmatrix}\mu^z_{ge}\mu^z_{eg} & \mu^z_{ge}\mu^y_{eg} \\ \mu^y_{ge}\mu^z_{eg} & \mu^y_{ge}\mu^y_{eg}\end{bmatrix} = \frac{e^2}{|\beta d_1|^2 + |\alpha d_3|^2}\begin{bmatrix}|\alpha|^2|d_3|^4 & \mathrm{e}^{i\Omega\Delta t}\beta^*\alpha|d_1|^2|d_3|^2 \\ \mathrm{e}^{-i\Omega\Delta t}\beta\alpha^*|d_1|^2|d_3|^2 & |\beta|^2|d_1|^4\end{bmatrix} \tag{3.34}$$

One obtains the eigenvalues $\lambda_1 = 0$ and $\lambda_2 = |\beta|^2|d_1|^4 + |\alpha|^2|d_3|^4$ after diagonalization of the latter matrix, i.e. solving

$$\begin{vmatrix} |\alpha|^2|d_3|^4-\lambda & \mathrm{e}^{i\Omega\Delta t}\beta^*\alpha|d_1|^2|d_3|^2 \\ \mathrm{e}^{-i\Omega\Delta t}\beta\alpha^*|d_1|^2|d_3|^2 & |\beta|^2|d_1|^4-\lambda \end{vmatrix}=0 \tag{3.35}$$

The corresponding (normalized) eigenvectors $\hat{\mathbf{z}}'$ and $\hat{\mathbf{y}}'$ are the principal axes that we are looking for. For $\lambda_1=0$ we have

$$\begin{bmatrix} |\alpha|^2|d_3|^4 & \mathrm{e}^{i\Omega\Delta t}\beta^*\alpha|d_1|^2|d_3|^2 \\ \mathrm{e}^{-i\Omega\Delta t}\beta\alpha^*|d_1|^2|d_3|^2 & |\beta|^2|d_1|^4 \end{bmatrix}\begin{bmatrix} z_1' \\ z_2' \end{bmatrix}=0 \tag{3.36}$$

which implies

$$\frac{z_1'}{z_2'}=-\mathrm{e}^{i\Omega\Delta t}\frac{\beta^*|d_1|^2}{\alpha^*|d_3|^2} \tag{3.37}$$

Normalization yields for the first principal axis

$$\hat{\mathbf{z}}'=\frac{-\mathrm{e}^{i\Omega\Delta t}\beta^*|d_1|^2\hat{\mathbf{z}}+\alpha^*|d_3|^2\hat{\mathbf{y}}}{\sqrt{|\beta|^2|d_1|^4+|\alpha|^2|d_3|^4}} \tag{3.38}$$

which is clearly time-dependent. For $\lambda_2=|\beta|^2|d_1|^4+|\alpha|^2|d_3|^4$ we have

$$\begin{bmatrix} -|\beta|^2|d_1|^4 & \mathrm{e}^{i\Omega\Delta t}\beta^*\alpha|d_1|^2|d_3|^2 \\ \mathrm{e}^{-i\Omega\Delta t}\beta\alpha^*|d_1|^2|d_3|^2 & -|\alpha|^2|d_3|^4 \end{bmatrix}\begin{bmatrix} y_1' \\ y_2' \end{bmatrix}=0 \tag{3.39}$$

which implies

$$\frac{y_1'}{y_2'}=\mathrm{e}^{i\Omega\Delta t}\frac{\alpha|d_3|^2}{\beta|d_1|^2} \tag{3.40}$$

Normalization yields for the second time-dependent principal axis

$$\hat{\mathbf{y}}'=\frac{\mathrm{e}^{i\Omega\Delta t}\alpha|d_3|^2\hat{\mathbf{z}}+\beta|d_1|^2\hat{\mathbf{y}}}{\sqrt{|\beta|^2|d_1|^4+|\alpha|^2|d_3|^4}} \tag{3.41}$$

Note that the third principal axis $\hat{\mathbf{x}}$ remains unaffected (if the x-component of $\mathbf{E}_{pump}$ equals zero) and will therefore not be taken into account anymore. Determining the polarization of the probe pulse upon transmission is based on determining the refractive indices of these time-dependent principal axes. In the inertial frame of these principal axes, i.e. the $\{\hat{\mathbf{z}}',\hat{\mathbf{y}}'\}$-basis, the only nonzero element of $\tilde{\boldsymbol{\chi}}^{(1)}$ is the eigenvalue

$$\tilde{\chi}^{(1)}_{y'y'}=\frac{N}{\varepsilon_0\hbar}\mu^{y'}_{ge}\mu^{y'}_{eg}\frac{\Delta_p-i\gamma}{\Delta_p^2+\gamma^2} \tag{3.42}$$

where

$$\mu_{ge}^{y'}\mu_{eg}^{y'} = e^2\frac{|\beta|^2|d_1|^4 + |\alpha|^2|d_3|^4}{|\beta d_1|^2 + |\alpha d_3|^2} \tag{3.43}$$

In general, the complex refractive index of principal axis $\hat{\mathbf{j}}$ is given by

$$\tilde{n}_j = \sqrt{1 + \tilde{\chi}_{jj}^{(1)}} \approx 1 + \frac{1}{2}\tilde{\chi}_{jj}^{(1)} \tag{3.44}$$

where the latter approximation is valid for $\left|\tilde{\chi}_{jj}^{(1)}\right| << 1$. In our case we have $\tilde{n}_{y'} \approx 1 + \frac{1}{2}\tilde{\chi}_{y'y'}^{(1)}$ and $\tilde{n}_{z'} = 1$. Since the refractive index differs in one direction, the sample behaves as a (singly) birefringent material. To describe how the probe pulse is affected by the sample, one should consider the Jones matrix $J\{\hat{\mathbf{z}}, \hat{\mathbf{y}}\}$, which performs the following transformation

$$\mathbf{E}_{out}\{\hat{\mathbf{z}}, \hat{\mathbf{y}}\} = J\{\hat{\mathbf{z}}, \hat{\mathbf{y}}\}\mathbf{E}_{in}\{\hat{\mathbf{z}}, \hat{\mathbf{y}}\} = J\{\hat{\mathbf{z}}, \hat{\mathbf{y}}\}\begin{bmatrix}\delta \\ \varepsilon\end{bmatrix} \tag{3.45}$$

To build $J\{\hat{\mathbf{z}}, \hat{\mathbf{y}}\}$ we first build $J\{\hat{\mathbf{z}}', \hat{\mathbf{y}}'\}$, which describes how a probe pulse in the $\{\hat{\mathbf{z}}', \hat{\mathbf{y}}'\}$-basis is affected, i.e.

$$\mathbf{E}_{out}\{\hat{\mathbf{z}}', \hat{\mathbf{y}}'\} = J\{\hat{\mathbf{z}}', \hat{\mathbf{y}}'\}\mathbf{E}_{in}\{\hat{\mathbf{z}}', \hat{\mathbf{y}}'\} \tag{3.46}$$

The Jones matrix is given by

$$J\{\hat{\mathbf{z}}', \hat{\mathbf{y}}'\} = \begin{bmatrix}\mathrm{e}^{i\Lambda n_{z'}} & 0 \\ 0 & \mathrm{e}^{i\Lambda n_{y'}}\end{bmatrix} \tag{3.47}$$

which expresses the retardation of (light polarized along) principal axis $\hat{\mathbf{j}}$ by Λn_j where $\Lambda \equiv 2\pi d/\lambda$, with d the thickness of the sample and λ the wavelength of the light[16]. Note that we consider here only the real part of the complex refractive index, which is valid for a sufficiently detuned probe pulse. In Section 3.7 we therefore required $|\Delta_p| >> \gamma$, implying $\frac{\Delta_p - i\gamma}{\Delta_p^2+\gamma^2} \approx \Delta_p^{-1}$. It is convenient to define

$$\Delta n \equiv n_{y'} - n_{z'} \approx \frac{N}{2\varepsilon_0\hbar\Delta_p}e^2\frac{|\beta|^2|d_1|^4 + |\alpha|^2|d_3|^4}{|\beta d_1|^2 + |\alpha d_3|^2} \tag{3.48}$$

Multiplication of the Jones matrix with the global phase factor $\mathrm{e}^{-i\Lambda n_{z'}}$ gives

$$J\{\hat{\mathbf{z}}', \hat{\mathbf{y}}'\} = \begin{bmatrix}1 & 0 \\ 0 & \mathrm{e}^{i\Lambda\Delta n}\end{bmatrix} \tag{3.49}$$

The eigenvectors of the Jones matrix are called eigenpolarizations, which are equivalent to the principal axes. As it should, the Jones matrix in Eq. (3.47) satisfies the requirement that the eigenpolarizations correspond to the two polarization states that pass through the optical system unaffected[16]. However, since the polarizations have different retardations, the resulting polarization of a passing light pulse consisting of a superposition of the principal axes might be affected. In this work, polarization rotation is considered in particular, which implies for linearly polarized light a rotation of the plane in which the electric field component oscillates.

The Jones matrix $J\{\hat{\mathbf{z}},\hat{\mathbf{y}}\}$ is obtained using the transformation matrix T which has as its columns the unit vectors $\hat{\mathbf{z}}'\{\hat{\mathbf{z}},\hat{\mathbf{y}}\}$ (Eq. 3.38) and $\hat{\mathbf{y}}'\{\hat{\mathbf{z}},\hat{\mathbf{y}}\}$ (Eq. 3.41), respectively. Let us build the matrices T and $T^\dagger$ that perform a transformation from the $\{\hat{\mathbf{z}}',\hat{\mathbf{y}}'\}$-basis to the $\{\hat{\mathbf{z}},\hat{\mathbf{y}}\}$-basis and back, respectively.

$$T = \frac{1}{\sqrt{|\beta|^2|d_1|^4+|\alpha|^2|d_3|^4}}\begin{bmatrix} -\mathrm{e}^{i\Omega\Delta t}\beta^*|d_1|^2 & \mathrm{e}^{i\Omega\Delta t}\alpha|d_3|^2 \\ \alpha^*|d_3|^2 & \beta|d_1|^2 \end{bmatrix} \tag{3.50}$$

where the conjugate transpose is given by

$$T^\dagger = \frac{1}{\sqrt{|\beta|^2|d_1|^4+|\alpha|^2|d_3|^4}}\begin{bmatrix} -\mathrm{e}^{-i\Omega\Delta t}\beta|d_1|^2 & \alpha|d_3|^2 \\ \mathrm{e}^{-i\Omega\Delta t}\alpha^*|d_3|^2 & \beta^*|d_1|^2 \end{bmatrix} \tag{3.51}$$

of which the columns consist of the unit vectors $\hat{\mathbf{z}}\{\hat{\mathbf{z}}',\hat{\mathbf{y}}'\}$ and $\hat{\mathbf{y}}\{\hat{\mathbf{z}}',\hat{\mathbf{y}}'\}$, respectively, i.e.

$$\hat{\mathbf{z}} = \mathrm{e}^{-i\Omega\Delta t}\frac{-\beta|d_1|^2\hat{\mathbf{z}}'+\alpha^*|d_3|^2\hat{\mathbf{y}}'}{\sqrt{|\beta|^2|d_1|^4+|\alpha|^2|d_3|^4}} \tag{3.52}$$

$$\hat{\mathbf{y}} = \frac{\alpha|d_3|^2\hat{\mathbf{z}}'+\beta^*|d_1|^2\hat{\mathbf{y}}'}{\sqrt{|\beta|^2|d_1|^4+|\alpha|^2|d_3|^4}} \tag{3.53}$$

Altogether the Jones matrix of Eq. (3.45) becomes

$$\begin{aligned} J\{\hat{\mathbf{z}},\hat{\mathbf{y}}\} &= TJ\{\hat{\mathbf{z}}',\hat{\mathbf{y}}'\}T^\dagger \\ &= j_0\begin{bmatrix} -\mathrm{e}^{i\Omega\Delta t}\beta^*|d_1|^2 & \mathrm{e}^{i\Omega\Delta t}\alpha|d_3|^2 \\ \alpha^*|d_3|^2 & \beta|d_1|^2 \end{bmatrix}\begin{bmatrix} 1 & 0 \\ 0 & \mathrm{e}^{i\Lambda\Delta n} \end{bmatrix}\begin{bmatrix} -\mathrm{e}^{-i\Omega\Delta t}\beta|d_1|^2 & \alpha|d_3|^2 \\ \mathrm{e}^{-i\Omega\Delta t}\alpha^*|d_3|^2 & \beta^*|d_1|^2 \end{bmatrix} \\ &= j_0\begin{bmatrix} j_{zz} & j_{zy} \\ j_{yz} & j_{yy} \end{bmatrix} \end{aligned} \tag{3.54}$$

where

$$\begin{aligned}
j_0 &\equiv \frac{1}{|\beta|^2|d_1|^4 + |\alpha|^2|d_3|^4} \\
j_{zz} &\equiv \mathrm{e}^{i\Lambda\Delta n}|\alpha|^2|d_3|^4 + |\beta|^2|d_1|^4 \\
j_{zy} &\equiv \mathrm{e}^{i\Omega\Delta t}\left(\mathrm{e}^{i\Lambda\Delta n} - 1\right)\beta^*\alpha|d_1|^2|d_3|^2 \\
j_{yz} &\equiv \mathrm{e}^{-i\Omega\Delta t}\left(\mathrm{e}^{i\Lambda\Delta n} - 1\right)\beta\alpha^*|d_1|^2|d_3|^2 \\
j_{yy} &\equiv \mathrm{e}^{i\Lambda\Delta n}|\beta|^2|d_1|^4 + |\alpha|^2|d_3|^4
\end{aligned} \tag{3.55}$$

Substitution into Eq. (3.45) yields the following components

$$\begin{aligned}
E_{out,z} &= j_0\left(\mathrm{e}^{i\Omega\Delta t}\left(\mathrm{e}^{i\Lambda\Delta n} - 1\right)P_1 + \mathrm{e}^{i\Lambda\Delta n}P_2 + P_3\right) \\
E_{out,y} &= j_0\left(\mathrm{e}^{-i\Omega\Delta t}\left(\mathrm{e}^{i\Lambda\Delta n} - 1\right)Q_1 + \mathrm{e}^{i\Lambda\Delta n}Q_2 + Q_3\right)
\end{aligned} \tag{3.56}$$

with

$$\begin{aligned}
P_1 &= \beta^*\alpha\varepsilon|d_1|^2|d_3|^2 \\
Q_1 &= \beta\alpha^*\delta|d_1|^2|d_3|^2 \\
P_2 &= |\alpha|^2\delta|d_3|^4 \\
Q_2 &= |\beta|^2\varepsilon|d_1|^4 \\
P_3 &= |\beta|^2\delta|d_1|^4 \\
Q_3 &= |\alpha|^2\varepsilon|d_3|^4
\end{aligned}$$

To determine the polarization rotation we follow the Cartesian complex-plane representation of polarized light, according to the book of Azzam and Bashara[16]. Using Eq. (1.77) of [16], we define the ratio

$$\kappa = E_y/E_z \tag{3.57}$$

where we use κ in contrast to [16] (which uses χ). In line with Eq. (1.86) of [16], we adopt the expression for the azimuth θ

$$\tan(2\theta) = \frac{2\,\mathrm{Re}\{\kappa\}}{1 - |\kappa|^2} \tag{3.58}$$

which implies

$$\theta = \frac{1}{2}\tan^{-1}\left(\frac{\kappa^* + \kappa}{1 - \kappa^*\kappa}\right) \tag{3.59}$$

Note that the $\tan^{-1}$ function returns a value in the range $(-\pi/2, \pi/2)$. In practice therefore, to return a value for θ in the range $(-\pi, \pi]$, we actually use the atan2 function (as implemented in most programming languages), i.e.

$$\theta = \frac{1}{2}\,\mathrm{atan}\,2\left(\kappa^* + \kappa, 1 - \kappa^*\kappa\right) \tag{3.60}$$

The polarization rotation (optical rotation angle) $\Delta\theta$ is now given by

$$\Delta\theta = \theta_{out} - \theta_{in} \tag{3.61}$$

From Eq. (1.87) of [16] we obtain for the ellipticity angle ϵ

$$\sin(2\epsilon) = \frac{2\,\mathrm{Im}\{\kappa\}}{1+|\kappa|^2} \tag{3.62}$$

which implies

$$\epsilon = \frac{1}{2}\sin^{-1}\left(i\frac{\kappa^* - \kappa}{1+\kappa^*\kappa}\right) \tag{3.63}$$

3.9 SI: Idealized TRFR scenario for a V-system

Let us consider the simplest model example (with reference to main text Fig. 3.2) that satisfies the conditions for the TRFR experiment, i.e. transition dipole moments $d_1 = d_3 \equiv d_0$ and real-valued $\alpha = \beta = \delta = \varepsilon \equiv E_0/\sqrt{2}$, i.e. $\mathbf{E}_{pump} = \mathbf{E}_{in} = E_0\frac{\hat{\mathbf{z}}+\hat{\mathbf{y}}}{\sqrt{2}}$ (main text Fig. 3.1). From Eq. (3.28) it follows that

$$|\psi_e(t)\rangle = \frac{|\psi_1\rangle + \mathrm{e}^{i\Omega t}|\psi_3\rangle}{\sqrt{2}} \tag{3.64}$$

with $\Omega \equiv \omega_{13} = (E_1 - E_3)/\hbar$. Assuming that ω_p is nearly resonant with the transition from $|\psi_e(t)\rangle$ to $|\psi_g\rangle$, i.e. with the transition frequency $\omega_{ge} = (E_g - E_e)/\hbar < 0$, the only nonzero eigenvalue of $\tilde{\boldsymbol{\chi}}^{(1)}$ is to a good approximation given by[54]

$$\tilde{\chi}^{(1)}_{y'y'}(\omega_p) \approx \frac{N}{\varepsilon_0\hbar}e^2|d_0|^2\frac{\Delta_p - i\gamma}{\Delta_p^2 + \gamma^2} \tag{3.65}$$

where the tilde denotes a complex number, $\Delta_p = \omega_{ge} + \omega_p$ the detuning and γ the damping rate. The eigenvectors of $\tilde{\boldsymbol{\chi}}^{(1)}$ are the principal axes

$$\hat{\mathbf{z}}' = \frac{\mathrm{e}^{i\Omega\Delta t}\hat{\mathbf{z}} + \hat{\mathbf{y}}}{\sqrt{2}} \tag{3.66}$$

$$\hat{\mathbf{y}}' = \frac{-\mathrm{e}^{i\Omega\Delta t}\hat{\mathbf{z}} + \hat{\mathbf{y}}}{\sqrt{2}} \tag{3.67}$$

as obtained from Eq. (3.38) and (3.41), respectively. The polarization of the probe pulse upon transmission (to which we refer as the outcoming probe) is given by Eq. (3.56), which for this idealized scenario becomes

$$\mathbf{E}_{out}\{\hat{\mathbf{z}},\hat{\mathbf{y}}\} = \frac{E_0}{2\sqrt{2}}\begin{bmatrix}\mathrm{e}^{i\Omega\Delta t}\left(\mathrm{e}^{i\Lambda\Delta n} - 1\right) + \mathrm{e}^{i\Lambda\Delta n} + 1 \\ \mathrm{e}^{-i\Omega\Delta t}\left(\mathrm{e}^{i\Lambda\Delta n} - 1\right) + \mathrm{e}^{i\Lambda\Delta n} + 1\end{bmatrix} \tag{3.68}$$

where $\Lambda \equiv 2\pi d/\lambda$, d the thickness of the sample, λ the wavelength of the light, and $\Delta n \approx \mathrm{Re}\left\{\tilde{\chi}^{(1)}_{y'y'}\right\}/2$ as follows from Eq. (3.48).

At one and three quarters of the period of oscillation $P = 2\pi/\Omega$ (or at any multiple of P later), the principal axes are circular. Let us consider the case $\Delta t = \frac{1}{4}P$ with principal axes

$$\hat{\mathbf{z}}'(\Delta t = \frac{1}{4}P) = \frac{i\hat{\mathbf{z}} + \hat{\mathbf{y}}}{\sqrt{2}} \tag{3.69}$$

$$\hat{\mathbf{y}}'(\Delta t = \frac{1}{4}P) = \frac{-i\hat{\mathbf{z}} + \hat{\mathbf{y}}}{\sqrt{2}} \tag{3.70}$$

Since these circular principal axes experience different refractive indices, the polarization of a linear probe pulse will be (maximally) rotated upon interaction with the sample when the probe pulse arrives at delay time $\Delta t = \frac{1}{4}P$. To derive the expression for the optical rotation angle, $\Delta t = \frac{1}{4}P$ is substituted into Eq. (3.68), which yields the following real components after multiplication with the global phase factor $\mathrm{e}^{-i\Lambda\Delta n/2}$

$$E_{z,out}(\Delta t = \frac{1}{4}P) = E_0 \cos\left(\frac{\Lambda\Delta n}{2} + \frac{\pi}{4}\right) \tag{3.71}$$

$$E_{y,out}(\Delta t = \frac{1}{4}P) = E_0 \sin\left(\frac{\Lambda\Delta n}{2} + \frac{\pi}{4}\right) \tag{3.72}$$

For the case of a Jones vector with real components, the azimuth θ is directly obtained from

$$\theta = \tan^{-1}\left(\frac{E_y}{E_z}\right) \tag{3.73}$$

With the electric vector of the incoming probe given by $\mathbf{E}_{in} = E_0\frac{\hat{\mathbf{z}}+\hat{\mathbf{y}}}{\sqrt{2}}$, and the outcoming probe pulse by Eq. (3.71) and (3.72), the optical rotation angle at $\Delta t = \frac{1}{4}P$ is given by

$$\begin{aligned}\Delta\theta_{max} &= \tan^{-1}\left(\frac{\sin\left(\frac{\Lambda\Delta n}{2} + \frac{\pi}{4}\right)}{\cos\left(\frac{\Lambda\Delta n}{2} + \frac{\pi}{4}\right)}\right) - \frac{\pi}{4} \\ &= \frac{\Lambda\Delta n}{2} = \frac{\pi d\Delta n}{\lambda}\end{aligned} \tag{3.74}$$

This is the well-known expression for the optical rotation angle of linearly polarized light in case of circular principal axes. Analogously, at $\Delta t = \frac{3}{4}P$, one finds $\Delta\theta = -\Delta\theta_{max}$.

3.10 SI: TRFR model results and discussion

As long as the polarization of the probe remains to a good approximation linear (i.e. small ellipticity angle), $\Delta\theta$ behaves as a sinusoid with angular frequency Ω and amplitude $\Delta\theta_{max}$ as a function of the delay time Δt. See main text Fig. 3.4 for an example of such oscillation of $\Delta\theta$, using the following input parameters: Polarization parameters $\alpha = \beta = \delta = \varepsilon = 1/\sqrt{2}$, i.e. $\hat{\mathbf{E}}_{pump} = \hat{\mathbf{E}}_{in} = \frac{\hat{\mathbf{z}}+\hat{\mathbf{y}}}{\sqrt{2}}$; Transition dipole moments $d_1 = 0.0003 - i0.0112$ and $d_3 = 0.0063$ (atomic units); Triplet sublevel splitting $E_3 - E_1 = 20$ meV (30 THz angular frequency); Probe wavelength $\lambda = 349$ nm ($\frac{\omega_p}{2\pi} = 846$ THz) based on $E_e - E_g = 3.55$ eV; Detuning $\Delta_p = -60$ meV $= 14.5$ THz. Note that this value is assumed to satisfy the requirements $|\Delta_p| >> \gamma$ and $|\Delta_p| >> |E_3 - E_1|/\hbar$ (Section 3.7). Also, we neglect the effect of detuning on λ (the probe's wavelength) since it amounts only 1.7% of the probe's frequency; Sample thickness $d = 100$ nm; Number density $N = 10^{24}$ m^{-3}, corresponding to 1 molecule per 1000 nm^3. This is considered to be small enough to prevent the molecules from affecting each other, given that the length of the molecule is 7.5 Å along the C_2-axis (main text Fig. 3.1), according to the scalar relativistic calculation of the ground state geometry (Table 3.1 (right)). This number density corresponds to on average 1 molecule per 10 nm, i.e. 10 molecules along the thickness d.

Substituting these parameters into Eq. (3.42) gives $\mathrm{Re}\left\{\tilde{\chi}^{(1)}_{y'y'}\right\} \approx -8.92 \cdot 10^{-8}$ for which the absolute value is much smaller than 1, which allows to use Eq. (3.44) for the approximation of $n_{y'}$. Using Eq. (3.48), we obtain $\Delta n = \mathrm{Re}\left\{\tilde{\chi}^{(1)}_{y'y'}\right\}/2 \approx -4.46 \cdot 10^{-8}$, which is substituted into Eq. (3.56). Following Eq. (3.57)−(3.61), we calculate $\Delta\theta(\Delta t)$, as is depicted in main text Fig. 3.4. The ellipticity angle of the outcoming probe is calculated with Eq. (3.63). The ellipticity angle change is given by $\Delta\epsilon = \epsilon_{out} - \epsilon_{in}$. Since the incoming probe is linear, we have $\epsilon_{in} = 0$. The ellipticity angle change turns out to be constant as a function of Δt, i.e. $\Delta\epsilon \approx -3.28 \cdot 10^{-8}$ rad. Moreover, this change turns out to be small enough, to be allowed to assume that the outcoming probe pulse remains linear. This follows from calculating

$$\theta_{out} \approx \tan^{-1}\left(\frac{|E_{out,y}|}{|E_{out,z}|}\right) \tag{3.75}$$

which to a good approximation equals the exact calculation of Eq. (3.59). Eq. (3.75) also illustrates for the case of a small ellipticity angle change, that the azimuth can be determined experimentally by simply measuring the intensity of the outcoming probe in the directions $\hat{\mathbf{y}}$ and $\hat{\mathbf{z}}$, i.e.

$$\theta_{out} \approx \tan^{-1}\left(\sqrt{\frac{I_y}{I_z}}\right) \tag{3.76}$$

Let us consider the ideal scenario ($d_1 = d_3$ and real-valued $\alpha = \beta = \delta = \varepsilon$), to evaluate some pathways to come up with an ideal molecular sample for a TRFR experiment. The signal is affected by different parameters, of which we consider the ones that can be adjusted relatively easily:

(i) $\Delta\theta$ is proportional to Δn (Eq. (3.74)), which is proportional to the linear susceptibility (Eq. (3.65)) and depends therefore quadratically on the transition dipole moment (and thus linearly on the oscillator strength). Taking a molecule with larger transition dipole moments (which requires larger SOC) will thus significantly increase the amplitude of oscillation. One should keep in mind here that the probability for exciton recombination also increases with increasing transition dipole moments, which implies a decreasing lifetime. Hence, the most suitable molecule for a TRFR experiment satisfies a trade-off between a) large enough SOC to be able to measure $\Delta\theta$, and b) not too large SOC in order to have large lifetime.

(ii) $\Delta\theta$ depends linearly on the number density N, since Δn (Eq. (3.74)) is proportional to N.

(iii) $\Delta\theta$ depends linearly on the thickness d (Eq. (3.74)).

(iv) $\Delta\theta$ depends strongly on the detuning Δ_p, since $\Delta\theta$ is proportional to $\frac{\Delta_p}{\Delta_p^2+\gamma^2}$, which equals approximately Δ_p^{-1} for $|\Delta_p| >> \gamma$ (which is required to prevent population transfer). Since we take $\Delta_p = 3(E_3 - E_1)$ (assumed to satisfy equal detuning for both sublevels), we can increase the signal by decreasing the energy splitting (as long as $|\Delta_p| >> \gamma$ is satisfied). Since we consider isolated molecules that individually contribute to the total TRFR signal, we should consider single molecules for typical values of the damping rate γ. In general, the width of an absorption line is given by two times γ. Typical absorption line widths of single molecules are in the order of (tens of) MHz[64]. As a rule of thumb, the order of magnitude of the energy splitting for a molecular TRFR experiment should thus be at least 100 MHz. Regarding Δ_p it is also useful to note that when working with an ensemble of systems it is wise to take $\Delta_p = \omega_{ge} + \omega_p$ negative, i.e. $\omega_p < |\omega_{ge}|$. The reason for this is that for positive Δ_p one might induce unwanted excitations with the probe for systems still having the ground state populated to an excited state that lies slightly above the lowest triplet state. Consequently, this reduces the intensity of the probe laser and the amplitude of the TRFR signal. However, if it is ensured that the vast majority of systems has been excited already (with an intense pump pulse), this will only have a small effect. When this effect is neglected, taking a detuning of $-\Delta_p$ shifts the TRFR signal half a period (main text Fig. 3.4) with respect to Δ_p. Here it is assumed again that we can neglect the effect of detuning on λ (the wavelength of the probe pulse) when substituting λ into Eq. (3.61) (through Eq. (3.56)) for the calculation of $\Delta\theta$.

Let us vary the input parameters to calculate how the signal ($\Delta\theta$) depends on them. Consider the same input parameters as in main text Fig. 3.4. For $PtN_2C_8H_{12}$ the calculated splitting between $|\psi_1\rangle$ and $|\psi_3\rangle$ is 4.8 THz. If we consider a splitting of 4.8 MHz instead, and $\gamma = 1$ MHz, we have $\mathrm{Re}\left\{\tilde{\chi}^{(1)}_{y'y'}\right\} \approx -0.089$. Since $\left|\mathrm{Re}\left\{\tilde{\chi}^{(1)}_{y'y'}\right\}\right| << 1$ is not valid now, we should take the exact expression for Δn, using the exact part of Eq. (3.44). The oscillation of $\Delta\theta(\Delta t)$ is still approximately sinusoidal, but the approximation of Eq. (3.75) deviates about 2.5% from using the exact Eq. (3.59). This deviation illustrates that the outcoming probe cannot be assumed to be linearly polarized anymore. This is directly reflected by the ellipticity angle change $\Delta\epsilon$, which as a function of Δt shows a sine with equilibrium value 0.034 rad and amplitude 0.4 mrad. However, 4.8 MHz does not satisfy our rule of thumb to take at least a splitting of 100 MHz, implying that $|\Delta_p| >> \gamma$ is usually not satisfied. Hence, one should expect to have a small signal lifetime due to population transfer to the ground state. Therefore, it will be very challenging to experimentally observe an oscillation of $\Delta\theta$ for a sample having such parameters.

The amplitudes of oscillation of both $\Delta\theta$ and $\Delta\epsilon$ become much larger when we besides increase the transition dipole moments. Taking it 10^2 times as large (molecules like e.g. $Ir(ppy)_3$[52] have such large transition dipole moments), together with a splitting 10^3 times as small with respect to the original parameters (main text Fig. 3.4), shows a non-sinusoidal behavior for $\Delta\theta$ and a nonzero equilibrium value. Still, $\Delta\epsilon$ oscillates sinusoidally. This illustrates that in the extreme case when we do not satisfy $\left|\mathrm{Re}\left\{\tilde{\chi}^{(1)}\right\}\right| << 1$, that the oscillation of $\Delta\theta$ is not suitable as a measure for the oscillation of $\langle \mathbf{J} \rangle (t)$, but one might consider to measure $\Delta\epsilon(\Delta t)$ instead.

We have shown that the TRFR experiment can be applied to molecules without using a magnetic field. This requires that there is a so-called zero-field splitting (ZFS), which is usually defined in terms of the so-called D- and E-parameter. In some cases one might want to perform the TRFR experiment at nonzero magnetic field, e.g. to study magnetic field dependence. Particularly interesting for this seem molecules with two sublevels of the lowest triplet excited state being degenerate ($E = 0$), combined with large transition dipole moments between the ground state and these sublevels. There are numerous examples of molecules with $E = 0$, while D is nonzero, i.e. the splitting between these sublevels and the third (e.g. Ir(ppy)$_3$[52]). The D-parameter directly depends on the amount of SOC. Depending on the symmetry of the molecule, E can be zero, which simultaneously allows to obtain large transition dipole moments by choosing a system with large SOC. One might now use a small magnetic field to slightly separate the degenerate sublevels. One should still ensure that the splitting is significantly larger than the damping rate γ.

When choosing a molecule for performing the TRFR experiment, one should also consider the following. Depending on the polarization and frequency of the light, one might excite to a superposition of more than two triplet sublevels. Consequently, the oscillation consists of a sum of sines with frequencies $|\omega_{ij}| = |E_i - E_j|/\hbar$ for levels for which $\langle\psi_i|\mathbf{J}|\psi_j\rangle$ is nonzero.

3.11 SI: Computational details and methods

In this work, we study as a function of time the oscillation of the polarization rotation $\Delta\theta$ and of the expectation value of the total angular momentum $\mathbf{J}$ for $PtN_2C_8H_{12}$ in case of a superposition of two triplet sublevels (Fig. 3.2a). The former requires i.a. the calculation of transition dipole moments between the ground state and excited state sublevels, whereas the latter also requires total angular momentum integrals. An accurate but costly way to calculate these is the use of the Complete Active Space SCF (CASSCF) and the second order perturbative correlation (CASPT2) methods combined with the restricted active space state interaction (RASSI) method to include SOC. This combined CASSCF/CASPT2/RASSI–SO method has been introduced by Roos and Malmqvist[17, 18].

To obtain the ground state geometry of $PtN_2C_8H_{12}$, a scalar relativistic density functional theory (DFT) calculation (using the one-component formulation of the zeroth-order regular approximation (ZORA)[65–68]) is performed with the Amsterdam Density Functional (ADF) program[31, 32], where the B3LYP[69] functional and TZP[70–72] basis set are used. According to this calculation, the lowest energy conformation of the molecule has C_2 symmetry (to which is referred as the C_2 geometry (Table 3.1 (left))), for which no imaginary frequencies are obtained. In view of computational efficiency for the CASSCF/CASPT2/RASSI–SO method however, the C_{2v} geometry (Table 3.1 (right)) is assumed to represent the ground state although it possesses two imaginary frequencies, i.e. $65i$ and $78i$ cm^{-1}, having symmetry b_1 and a_2, respectively, corresponding to vibrations that lower the symmetry from C_{2v} to C_s and C_2, respectively. This approach seems reasonable when the molecule is at room temperature, since the calculated energy difference between the two geometries amounts 22 meV. Also, the UV-Vis spectra for both geometries are calculated via time-dependent DFT (TDDFT)[73–76] (using ZORA) including SOC perturbatively[30]. No significant differences are obtained (Fig. 3.6). Hence, we conclude that we can safely assume the C_{2v} geometry for the ground state.

We have applied the CASSCF/CASPT2/RASSI–SO method to the $PtN_2C_8H_{12}$ molecule, using the MOLCAS[23] software using ANO-RCC[38, 77, 78] basis sets (contracted for Pt to $8s7p5d2f$, for N to $4s3p1d$, for C to $4s3p1d$, for H to $3s1p$) and the Douglas-Kroll method[79]. The first stage of the method is a CASSCF calculation. The selected CAS is given in Fig. 3.7, where also the labeling of the molecular orbitals (MOs) is explained. The lower lying inactive MOs are doubly occupied (31, 10, 5 and 21 MOs for the symmetries a_1, b_1, a_2 and b_2,

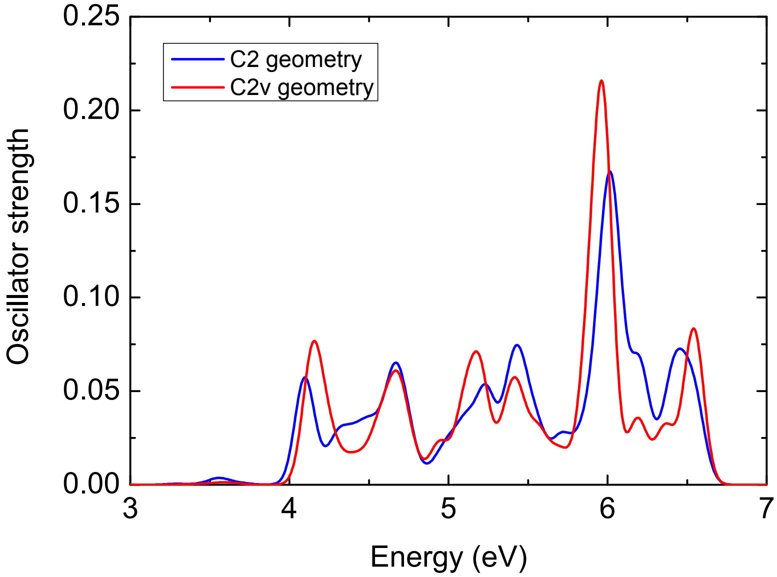

Figure 3.6: Excitation spectra as determined from TDDFT calculations, for the C_2 and C_{2v} geometry of $PtN_2C_8H_{12}$.

respectively). The Hartree-Fock configuration is $(1a_1)^2...(34a_1)^2(1b_1)^2...(13b_1)^2$ $(1a_2)^2...(7a_2)^2(1b_2)^2...(22b_2)^2$. Within our CASSCF calculation, 18 active electrons are distributed over 14 MOs. We have performed a state averaged CASSCF, calculating the 10 lowest roots for each symmetry. This results in 80 roots, which we call *spin-free* states in line with Molcas. The oscillator strengths between the excited *spin-free* states and the ground state 1^1A_1 are depicted in red in Fig. 3.8. Since SOC is not considered within this calculation, excitations from the singlet ground state can only take place to singlet excited states.

Using the CASSCF wave function, a CASPT2 calculation is performed to obtain a second order perturbation estimate of the correlation energy. The resulting energies are taken as an input for the RASSI method.

This work considers a direct excitation for $PtN_2C_8H_{12}$ when initially populated in the singlet ground state $|\psi_g\rangle$, to a superposition of two sublevels of the

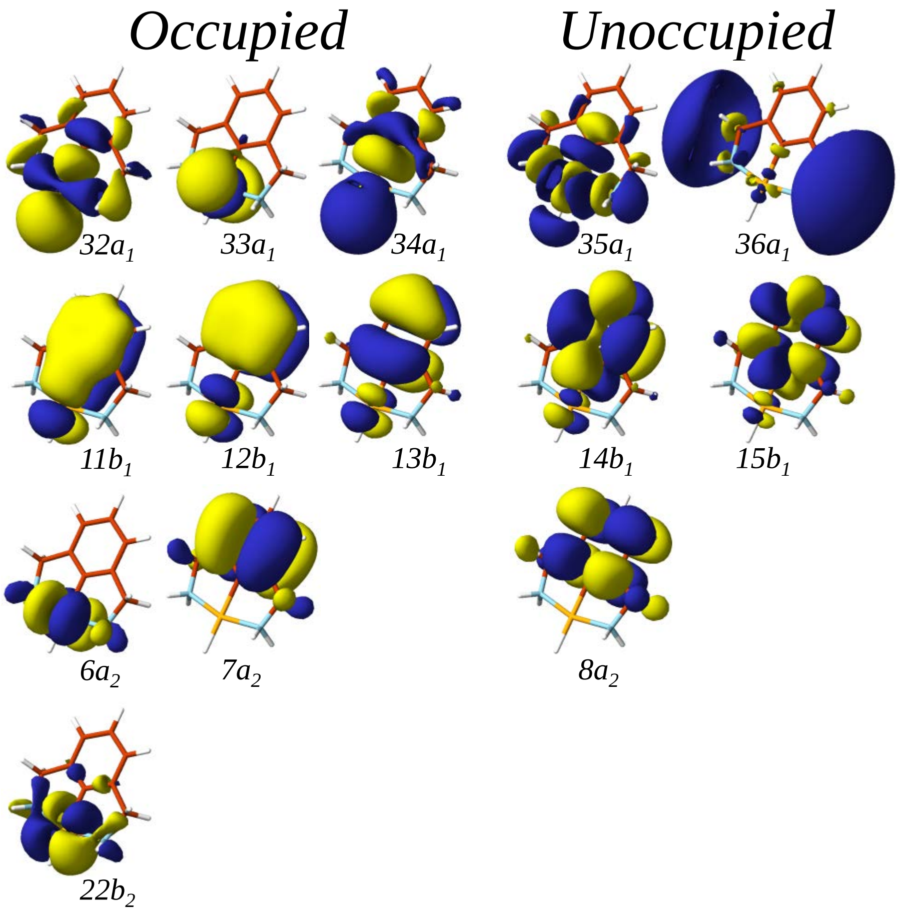

Figure 3.7: Selected molecular orbitals (MOs) for the Complete Active Space (CAS) of $PtN_2C_8H_{12}$.

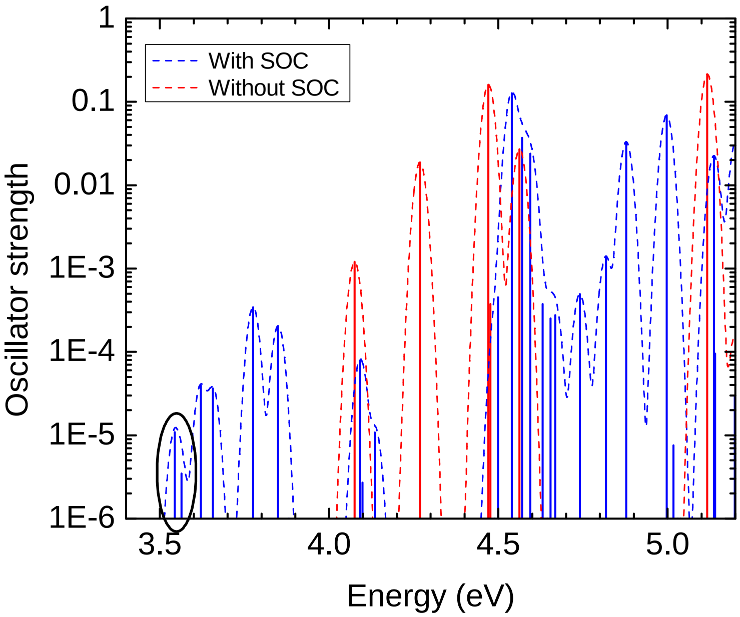

Figure 3.8: Excitation spectrum on semi-log scale, as obtained from ab initio calculations for the *spin-orbit* states (with SOC) and the *spin-free* states (without SOC). The height of the bars correspond to the oscillator strength for a transition from the ground state. The curves are intended as a guide to the eye, representing the excitation spectra broadened by Gaussians with $\sigma = 0.02$ eV. This work considers the lowest triplet (encircled), for which excitation is allowed to only two of the three sublevels (Fig. 3.9). Note that all nonzero f-values below 5.2 eV are contained in this plot.

lowest triplet excited state. SOC induces mixing of triplets into singlets and vice versa, which allows for excitations between them. In line with Molcas, we use the term *spin-orbit* to refer to the eigenbasis obtained after diagonalization of the Hamiltonian that includes the SOC term, which is performed within the RASSI method. Strictly speaking, because of the mixing one should not speak about singlet and triplet states anymore within the *spin-orbit* basis, but one usually does because the hybridised *spin-orbit* states often resemble the original *spin-free* states.

The RASSI calculation gives the *spin-orbit* states as a linear combination of *spin-free* states. Table 3.3 tabulates the main contributions of the four lowest *spin-orbit* states, where the corresponding transitions between MOs are tabulated in Table 3.2. Particularly interesting are the singlets mixed into the triplets and vice versa, since these are the contributions that give nonzero transition dipole moments between the ground and excited states and therefore enable a transition.

Table 3.1: Atomic coordinates (Å) for the C_2 (left) and C_{2v} (right) geometry of $PtN_2C_8H_{12}$.

Atom	X	Y	Z
Pt	0.000000	0.000000	-0.045142
N	-0.191499	2.057399	-0.390104
N	0.191499	-2.057399	-0.390104
C	0.000000	0.000000	-2.046215
C	-0.036646	-1.215345	-2.727430
C	0.036646	1.215345	-2.727430
C	0.026445	1.220441	-4.122237
C	-0.026445	-1.220441	-4.122237
C	0.000000	0.000000	-4.807534
C	0.143797	2.430631	-1.828603
C	-0.143797	-2.430631	-1.828603
H	0.000000	0.000000	-5.891159
H	0.047114	2.146972	-4.688039
H	-0.047114	-2.146972	-4.688039
H	-0.496914	3.257069	-2.147392
H	0.496914	-3.257069	-2.147392
H	1.170515	2.801231	-1.816104
H	-1.170515	-2.801231	-1.816104
H	1.164990	-2.276992	-0.194498
H	-1.164990	2.276992	-0.194498
H	-0.363756	-2.615608	0.250989
H	0.363756	2.615608	0.250989
H	0.000000	0.000000	1.623945

Atom	X	Y	Z
Pt	0.000000	0.000000	-0.046962
N	0.000000	2.066477	-0.365512
N	0.000000	-2.066477	-0.365512
C	0.000000	0.000000	-2.044076
C	0.000000	-1.215513	-2.727191
C	0.000000	1.215513	-2.727191
C	0.000000	1.219696	-4.122133
C	0.000000	-1.219696	-4.122133
C	0.000000	0.000000	-4.807861
C	0.000000	2.448529	-1.845813
C	0.000000	-2.448529	-1.845813
H	0.000000	0.000000	-5.891569
H	0.000000	2.146459	-4.688100
H	0.000000	-2.146459	-4.688100
H	-0.877938	3.072293	-2.029768
H	0.877938	3.072293	-2.029768
H	0.877938	-3.072293	-2.029768
H	-0.877938	-3.072293	-2.029768
H	0.811887	-2.467017	0.094995
H	-0.811887	-2.467017	0.094995
H	-0.811887	2.467017	0.094995
H	0.811887	2.467017	0.094995
H	0.000000	0.000000	1.624375

As can be seen in Table 3.3, *spin-orbit* state $|\psi_g\rangle$ has contributions from *spin-free* states 2^3B_2 and 1^3A_2, $|\psi_1\rangle$ from 1^1B_2, and $|\psi_3\rangle$ from 2^1A_1.

The oscillator strengths between the excited *spin-orbit* states and the ground state $|\psi_g\rangle$ are depicted in blue in Fig. 3.8. The oscillator strengths corresponding to the lowest triplet are encircled. The corresponding nonzero components of the transition dipole moments are $\langle\psi_1|\, y\, |\psi_g\rangle \approx 0.0003 - i0.0112$ and $\langle\psi_3|\, z\, |\psi_g\rangle \approx 0.0063$ in atomic units. In other words, a transition from $|\psi_g\rangle$ is allowed only with y and z polarized light to state $|\psi_1\rangle$ and $|\psi_3\rangle$ respectively, but forbidden to state $|\psi_2\rangle$ (Fig. 3.9).

Table 3.2: Lowest *spin-free* states (SFSs) for $PtN_2C_8H_{12}$. For the SFSs with important contributions to the states $|\psi_g\rangle$, $|\psi_1\rangle$, $|\psi_2\rangle$ and $|\psi_3\rangle$ (Table 3.3), the main MO configurations are given as well, corresponding to transitions between the MOs depicted in Fig. 3.7.

SFS	Energy (eV)	Conf., Weight	Conf., Weight
1^1A_1	0.00	Hartree-Fock, 0.92	
1^3B_1	3.78	$13b_1 \Rightarrow 35a_1$, 0.76	
1^3A_1	3.91	$13b_1 \Rightarrow 14b_1$, 0.42	$7a_2 \Rightarrow 8a_2$, 0.34
1^3A_2	3.99	$6a_2 \Rightarrow 35a_1$, 0.85	
2^3A_1	4.03	$33a_1 \Rightarrow 35a_1$, 0.77	
1^3B_2	4.06	$22b_2 \Rightarrow 35a_1$, 0.85	
1^1B_1	4.08	$13b_1 \Rightarrow 35a_1$, 0.65	
2^3B_2	4.18	$13b_1 \Rightarrow 8a_2$, 0.64	
2^1A_1	4.27	$33a_1 \Rightarrow 35a_1$, 0.80	
3^3A_1	4.42	$7a_2 \Rightarrow 8a_2$, 0.43	$13b_1 \Rightarrow 14b_1$, 0.33
3^1A_1	4.47	$34a_1 \Rightarrow 35a_1$, 0.53	$34a_1 \Rightarrow 36a_1$, 0.26
1^1B_2	4.48	$22b_2 \Rightarrow 35a_1$, 0.50	$13b_1 \Rightarrow 8a_2$, 0.21

Table 3.3: Main contributions for $PtN_2C_8H_{12}$ of the four lowest *spin-orbit* states (SOSs) in terms of the *spin-free* states (SFSs) for which the MO configurations are tabulated in Table 3.2.

SOS	Energy (eV)	SFS, Weight	SFS, Weight	SFS, Weight
$\|\psi_g\rangle$	0.00	1^1A_1, 0.97	2^3B_2, 0.015	1^3A_2, 0.0081
$\|\psi_1\rangle$	3.544	1^3B_1, 0.61	1^3A_1, 0.33	1^1B_2, 0.042
$\|\psi_2\rangle$	3.558	1^3B_1, 0.59	1^3A_1, 0.33	2^3B_2, 0.066
$\|\psi_3\rangle$	3.564	1^3B_1, 0.59 2^1A_1, 0.011	1^3A_2, 0.21	2^3B_2, 0.17

3.12 SI: Symmetry analysis

The aforementioned optical selection rules (Fig. 3.9) can also be obtained from group theoretical arguments. Here, we discuss two different approaches to come to the same conclusion.

Approach (1): The states $|\psi_1\rangle$, $|\psi_2\rangle$ and $|\psi_3\rangle$ mainly originate from *spin-free* state 1^3B_1 (Table 3.3). SOC has allowed this state to mix with singlets

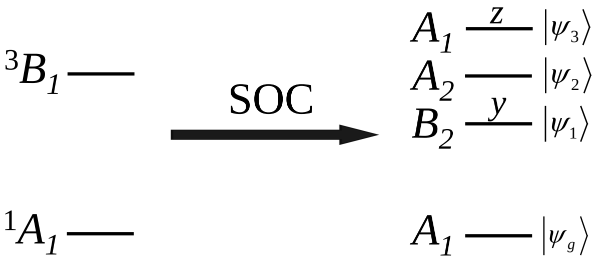

Figure 3.9: Energy diagram illustrating the effect of SOC on optical selection rules of originally forbidden singlet-triplet transitions. When SOC is not taken into account, the lowest triplet excited state of $PtN_2C_8H_{12}$ has B_1 symmetry. Due to SOC, three separate sublevels $|\psi_1\rangle$, $|\psi_2\rangle$ and $|\psi_3\rangle$ are obtained, having A_2, B_2 and A_1 symmetry, respectively. It is assumed here that the ground state has C_{2v} geometry. Excitations from the ground state can only take place to $|\psi_1\rangle$ and $|\psi_3\rangle$ with y and z polarized light respectively, whereas a transition to state $|\psi_2\rangle$ is forbidden.

having symmetry A_1, A_2 and B_2, as follows from the transformation of rotations, i.e. $B_2(R_x) + B_1(R_y) + A_2(R_z)$ within C_{2v}. Since the electric-dipole moment operator transforms as $B_1(x) + B_2(y) + A_1(z)$ within C_{2v}, it directly follows that excitations from the ground state are allowed to the lowest triplet only with y and z polarization (Fig. 3.9). Besides this contribution from singlets mixed into the lowest triplet (mainly 1^1B_2 for $|\psi_1\rangle$ and 2^1A_1 for $|\psi_3\rangle$), also triplets mixed into the ground state contribute to the mentioned transition dipole moments (mainly 2^3B_2 and 1^3A_2), as tabulated in Table 3.3.

Approach (2): The orbital part of the lowest triplet has B_1 symmetry. Let us now determine the symmetry of the triplet sublevels. In this regard it is convenient to consider the triplet spin functions T_x, T_y and T_z, defined as

$$T_x = \frac{T_{-1} - T_{+1}}{\sqrt{2}} = \frac{\beta_1\beta_2 - \alpha_1\alpha_2}{\sqrt{2}} \tag{3.77}$$

$$T_y = i\frac{T_{-1} + T_{+1}}{\sqrt{2}} = i\frac{\beta_1\beta_2 + \alpha_1\alpha_2}{\sqrt{2}} \tag{3.78}$$

$$T_z = T_0 = \frac{\alpha_1\beta_2 + \beta_1\alpha_2}{\sqrt{2}} \tag{3.79}$$

with α_i and β_i corresponding to the up and down spin of electron i respectively. T_x, T_y and T_z transform as rotations. For C_{2v} symmetry these are B_2, B_1 and A_2 for T_x, T_y and T_z, respectively. Taking the direct product between the orbital part (B_1) and the spin part (B_2, B_1 and A_2) implies that the sublevels have symmetry A_2, A_1 and B_2, respectively. To determine the possible excitations, one considers that x, y and z transform in C_{2v} as B_1, B_2 and A_1 respectively. From the A_1 ground state one can thus only excite to levels having symmetry B_1, B_2 and A_1, in order to let the integral $\langle\psi_e|\, D\, |\psi_g\rangle$ be nonzero. Hence, excitations from the ground state to the lowest triplet excited state can only take place for the B_2 and A_1 sublevels, when the system interacts with y and z polarized light respectively, whereas a transition to the B_1 sublevel is forbidden.

Table 3.4: FC-factors for 0-0 transition of different metal-organic molecules, as obtained from DFT calculations.

Molecule	FC-factor of 0-0 transition
$PtN_2C_8H_{12}$	$< 10^{-6}$
PtP (D_{4h} ground and excited state)	0.43
PtP (D_{4h} ground and C_{2h} excited state)	0.26
PtPπ (D_{4h} ground and excited state)	0.44

3.13 SI: Franck-Condon factors

The molecular TRFR experiment that we have introduced is based on measuring the triplet spin dynamics of a superposition of two electronic excited state sublevels (created by an on-resonance pump laser and probed via a probe laser that is slightly detuned with respect to the singlet-triplet transition). One should realize that electrons can couple to vibrations, implying that each electronic sublevel has a series of vibronic states. The Franck-Condon principle states that an electronic transition most likely occurs between vibronic states that have comparable geometry[35]. Creating and probing the excited state superposition is thus only possible if there is good vibrational overlap between the lowest vibronic sublevels of the electronic ground and excited state sublevels, for which the corresponding transition is commonly referred to as the 0-0 transition. In other words, the geometry should not distort too much upon excitation (within the timescale of the spin dynamics).

To study the geometry relaxation of the excited state, we have calculated the so-called Franck-Condon (FC) factors (a measure for the strength of a vibronic transition) for a series of vibronic states, of which we only report the 0-0 transition (for three molecules, Table 3.4). These FC-factors have been determined via DFT calculations with the ADF program[31, 32], using a B3LYP[69] functional and

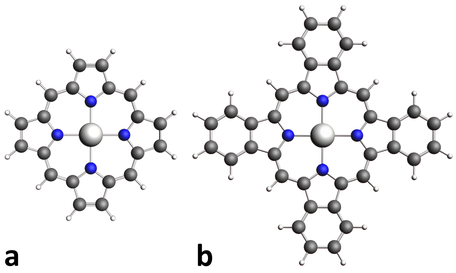

Figure 3.10: Platinum porphyrins, with **a**, an unsubstituted platinum porphyrin (PtP), and **b**, a π-extended platinum porphyrin (PtPπ). The platinum atom (white) is surrounded by nitrogen atoms (blue), which are surrounded by carbon (grey) and hydrogen (white) atoms.

TZP[70–72] basis set. Geometry optimizations and frequency calculations have been performed for both the singlet ground state (restricted DFT) and triplet excited state (unrestricted DFT).

Unfortunately, the geometry distortion turns out to be significant for the $PtN_2C_8H_{12}$ molecule that we consider in this work. This particularly follows from the fact that the FC-factor is extremely small for the 0-0 transition (Table 3.4). Although the detailed analysis for $PtN_2C_8H_{12}$ in our work is useful as a proof of principle for a molecular TRFR experiment, for a practical realization we should thus look for other candidate molecules.

The FC-factor of the 0-0 transition of a metal-organic molecule is typically large when the metal atom is well surrounded by the ligands. We found large FC-factors (Table 3.4) for the 0-0 transition of unsubstituted porphine platinum (to which we refer as PtP, Fig. 3.10a) and of a π-extended porphine platinum (to which we refer as PtPπ, Fig. 3.10b). Such a π-substitution is particularly interesting for manipulation of the transition energy of the molecule, since this wavelength was shown to increase (more than 200 nm) for an increasing number of fused-aromatic rings[80].

3.14 SI: Optical selection rules of platinum porphyrins

Platinum porphyrins are promising candidates for a molecular TRFR experiment. Diaconu et al. observed magnetic circular dichroism (different absorption for left and right circularly polarized light in a magnetic field) within the zero-phonon region of platinum porphyrins in organic hosts[45]. Their work summarizes polar-

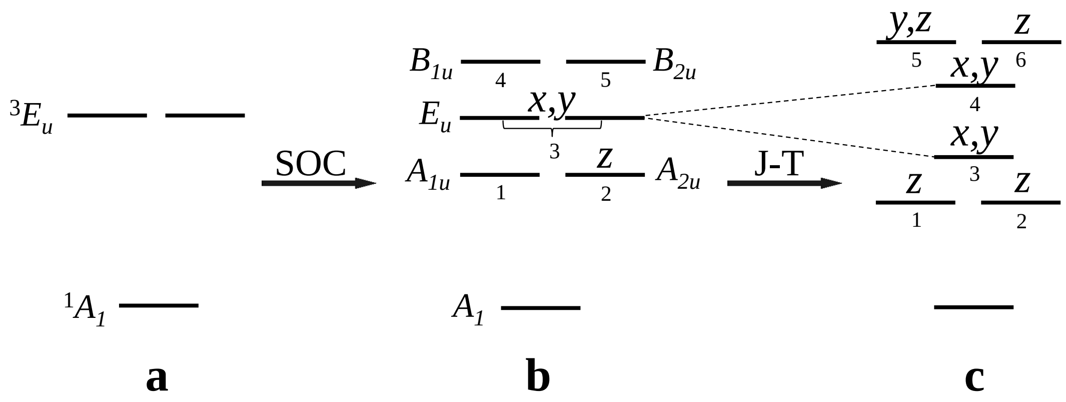

Figure 3.11: Energy diagram illustrating for PtP the effect of SOC and a Jahn-Teller (J-T) distortion on the optical selection rules of originally forbidden singlet-triplet transitions. **a**, When SOC is not taken into account, the lowest excited state of PtP is a doublet of two triplets with E_u symmetry, which according to our calculations originates from the molecular orbital excitation $a_{2u} \rightarrow e_g$. **b**, Due to SOC, a mixing of singlets and triplets occurs. Additionaly, the sublevels of the doublets split (labeled with a number (#) based on the energy (where 3 is a doublet) and their symmetry is depicted as well (within D_{4h})). Excitations from the ground state (D_{4h} geometry) can only take place to state 2 and 3 with z and (x, y) polarized light respectively, whereas the other transitions are forbidden (Table 3.5). **c**, After excitation, the system will undergo a Jahn-Teller distortion, which further splits the energy levels (Table 3.6) and the molecule gets C_{2h} symmetry.

ization selection rules that satisfy the criteria for a molecular TRFR experiment, and they present results with and without Jahn-Teller (J-T) and host interactions.

In order to study in more detail the optical transitions between the ground and excited state sublevels of PtP and PtPπ (Fig. 3.10), the CASSCF/CASPT2/-RASSI–SO method is not suitable, because of the relatively large number of atoms. Therefore, we perform TDDFT calculations (using ZORA) including SOC perturbatively[30]. These calculations are performed with ADF using a B3LYP functional and TZP basis set. In Table 3.5 we report for PtP (considering D_{4h} symmetry for both the ground and excited state geometry) the energies, oscillator strengths f and transition dipole moments μ, for the lowest 10 excitations from the ground state (from which the absorption spectrum can be derived).

When SOC is not taken into account, the lowest excited state of PtP is a doublet of two triplets with E_u symmetry, which according to our calculations originates from the molecular orbital excitation $a_{2u} \rightarrow e_g$. Instead, Diaconu *et*

Table 3.5: Transition dipole moments for the lowest 10 transitions from the ground state for PtP as obtained from TDDFT calculations, including SOC perturbatively (using ZORA). This calculation corresponds to the scheme in Fig. 3.11b (J-T distortion is still neglected). The oscillator strengths f and transition dipole moments μ determine the absorption spectrum of PtP, with their values given in atomic units (μ-values smaller than 10^{-5} are neglected). D_{4h} symmetry is considered. The excited states are labeled with a number (#) according to the energetic ordering. States 1-5 originate from a ^3E_u (which is a doublet of two triplets), and 6-10 from another ^3E_u. States 3 and 8 are each a degenerate doublet, which further split due to a Jahn-Teller distortion (Fig. 3.11c and Table 3.6).

#	Symm.	E (eV)	f	μ_x	μ_y	μ_z
1	A_{1u}	2.0189	0	0	0	0
2	A_{2u}	2.0190	$6.11 \cdot 10^{-8}$	0	0	$-i1.11 \cdot 10^{-3}$
3	E_u	2.0335	$1.65 \cdot 10^{-6}$	$i5.76 \cdot 10^{-3}$	0	0
4	B_{1u}	2.0486	0	0	0	0
5	B_{2u}	2.0488	0	0	0	0
6	A_{1u}	2.2202	0	0	0	0
7	A_{2u}	2.2202	$3.82 \cdot 10^{-8}$	0	0	$-i8.38 \cdot 10^{-4}$
8	E_u	2.2328	$2.96 \cdot 10^{-5}$	$i2.32 \cdot 10^{-2}$	0	0
9	B_{1u}	2.2457	0	0	0	0
10	B_{2u}	2.2457	0	0	0	0

al.[45] find as the lowest excited state the other close lying ^3E_u originating from $a_{1u} \rightarrow e_g$, which ends up as our second ^3E_u (consisting of states 6-10 in Table 3.5 when SOC is included, which gives quite comparable results).

Due to SOC, a mixing of singlets and triplets occurs. Additionaly, the sublevels of the doublets split, as depicted in Fig. 3.11b (with the sublevels labeled with a number (#) based on the energy (where 3 is a doublet) and their symmetry is depicted as well (within D_{4h})). Excitations from the ground state (D_{4h} geometry) can only take place to state 2 and 3 with z and (x, y) polarized light respectively, whereas the other transitions are forbidden (Table 3.5). The polarization selection rules obtained as such seem to be promising for a molecular TRFR experiment. A pump pulse polarized in both the z and (x, y) direction will induce a superposition between states 2 and 3, which can be probed via the polarization rotation upon transmission of a detuned probe pulse with similar polarization.

Table 3.6: Transition dipole moments for the lowest 6 transitions of PtP as obtained from spin-unrestricted TDDFT calculations with the excited state geometry taken as the ground state (to simulate the Jahn-Teller distortion), including SOC perturbatively (using ZORA). This calculation corresponds to the scheme in Fig. 3.11c. The oscillator strengths f and transition dipole moments μ determine the emission spectrum of PtP, with their values given in atomic units (μ-values smaller than 10^{-5} are neglected). No symmetry analysis is performed during the TDDFT calculation. The states are labeled with a number (#) according to the energetic ordering.

#	E (eV)	f	μ_x	μ_y	μ_z
1	1.7616	$1.08 \cdot 10^{-10}$	0	0	$4.99 \cdot 10^{-5}$
2	1.7617	$1.99 \cdot 10^{-8}$	0	0	$i6.79 \cdot 10^{-4}$
3	1.7622	$3.22 \cdot 10^{-6}$	$-8.10 \cdot 10^{-3}$ $+i7.56 \cdot 10^{-4}$	$-2.89 \cdot 10^{-3}$ $+i2.70 \cdot 10^{-4}$	0
4	1.9997	$9.98 \cdot 10^{-6}$	$-3.85 \cdot 10^{-3}$ $+i8.82 \cdot 10^{-4}$	$1.34 \cdot 10^{-2}$ $-i3.06 \cdot 10^{-3}$	0
5	2.0003	$3.18 \cdot 10^{-9}$	0	$i1.37 \cdot 10^{-5}$	$-4.06 \cdot 10^{-5}$ $+i2.51 \cdot 10^{-4}$
6	2.0004	$4.75 \cdot 10^{-9}$	0	0	$3.07 \cdot 10^{-4}$ $+i5.11 \cdot 10^{-5}$

However, one should be aware that after excitation with a pump pulse, the system undergoes a geometry relaxation (towards C_{2h}), i.e. a J-T distortion (Fig. 3.11c), which further splits the energy levels. This is no problem if the relaxation takes place on a longer time scale than the spin dynamics. If it takes place on a comparable timescale, the changes of the geometry and energy eigenstates should be small to prevent quantum decoherence. From the calculation of the FCFs we concluded already that the geometry change is relatively small (Section 3.13). We therefore expect only a small effect on the energies of the electronic states. To calculate the effect, we perform a spin-unrestricted TDDFT calculation with the triplet excited state geometry taken as the ground state geometry (Table 3.6). Such an approach is common in the calculation of emission spectra. The doublet E_u (Fig. 3.11b and Table 3.6) splits due to the J-T distortion. The optical selection rules for states $\#1-5$ in Table 3.5 and $\#1-6$ in Table 3.6 seem quite comparable, with more transitions allowed for the latter case however. In case the timescales of the J-T distortion and spin dynamics are comparable, the polarization rotation of the probe pulse is determined by

Table 3.7: Transition dipole moments for the lowest 10 transitions from the ground state (D_{4h} geometry) for PtPπ as obtained from TDDFT calculations, including SOC perturbatively (using ZORA). The oscillator strengths f and transition dipole moments μ determine the absorption spectrum of PtPπ, with their values given in atomic units (μ-values smaller than 10^{-5} are neglected). No symmetry restrictions are imposed during the TDDFT calculation. The excited states are labeled with a number (#) according to the energetic ordering. State 7 consists mainly of a singlet (the other states are mainly of triplet origin).

#	E (eV)	f	μ_x	μ_y	μ_z
1	1.46716	0	0	0	0
2	1.46716	0	0	0	0
3	1.46786	$3.60 \cdot 10^{-5}$	$-5.69 \cdot 10^{-4}$	$3.09 \cdot 10^{-2}$	0
4	1.70006	$1.85 \cdot 10^{-4}$	$-6.53 \cdot 10^{-2}$	$-1.10 \cdot 10^{-3}$	0
5	1.70136	0	0	0	0
6	1.70136	0	0	0	0
7	2.13466	0.2793	2.274	$3.70 \cdot 10^{-2}$	$-1.62 \cdot 10^{-5}$
8	2.20166	0	0	0	0
9	2.20176	0	0	0	0
10	2.20246	$1.50 \cdot 10^{-3}$	$1.64 \cdot 10^{-1}$	$2.60 \cdot 10^{-3}$	0

the transition dipole moments given in Table 3.6. After having created a superposition between states $\#2, 3$ in Table 3.5, the probe pulse should thus address (though slightly detuned to prevent population transfer back to the ground state) states $\#2, 3$ in Table 3.6. To quantify the change of states $\#2, 3$ (in Table 3.6 with respect to $\#2, 3$ in Table 3.5) it would be even more insightful to calculate the overlap of the eigenstates before and after the J-T distortion, which we have not done.

For a molecular TRFR experiment, the laser frequencies of the pump and probe pulse should match the singlet-triplet frequency. In that regard, for a TRFR experiment with platinum porphyrins the substitution of aromatic rings to PtP can be useful. We have performed similar TDDFT calculations for PtPπ (Table 3.7), which quite closely resemble the results of PtP. However, the fact that the transition dipole moment in the z-direction remains negligible for all states makes a TRFR experiment unpractical for PtPπ.

3.15 SI: Ensemble of randomly oriented molecules

In our calculations we have considered a sample consisting of an ensemble of similarly oriented molecules, illuminated at $t = 0$ with a linearly polarized pump pulse having polarization $\hat{\mathbf{E}}_{pump} = \frac{\hat{\mathbf{z}}+\hat{\mathbf{y}}}{\sqrt{2}}$ (with respect to the molecular frame of reference, as in main text Fig. 3.1). Let us address the following important conclusion: the TRFR signal decreases when the sample is rotated along any axis. In the molecular frame, the signal ultimately goes to zero when the electric vector oscillates only along x, y or z, simply because each system ends up in a single sublevel instead of a superposition. Interestingly, when the sample is rotated an angle ϕ along x (the propagation axis of the pump), the signal does not depend on ϕ if a circular instead of a linear pump is used, which might be experimentally favourable.

Instead of using an ensemble of similarly oriented molecules, we can consider the case of random orientations. One should keep in mind that for our derivation to be valid, the number density N should be small enough to ensure that the molecules are well isolated from each other. A particular example to which this section applies is the case of an ensemble of the molecule of interest put with random orientation in a crystalline host material. Perhaps even more interesting would be the case of a liquid host (i.e. in solution), or the molecule of interest put in the gas phase, since the molecules are then also well isolated. However, in these latter cases the signal might suffer from broadening due to the larger temperatures compared to the case of a crystalline host.

Let us consider a random ensemble of $PtN_2C_8H_{12}$ molecules, illuminated at $t = 0$ with a circular pump pulse (satisfying assumptions (*i*) to (*iv*) of Sec. 3.7, where $|\psi_e\rangle$ follows from Eq. (3.26)). Within this random ensemble, molecules having their plane parallel to the propagation axis will be excited to a single sublevel and do therefore not contribute to the TRFR signal. Instead, any molecule having its molecular plane exactly perpendicular to the pump propagation axis will be excited to a superposition of sublevels and does therefore contribute to the TRFR signal. At delay times where the signal is maximally positive or negative, these are the molecules that contribute most. At these times, all remaining molecules (having an orientation that is neither parallel nor perpendicular to the propagation axis) contribute to the total TRFR signal with a value that lies between zero and the maximum. Clearly, for an ensemble of randomly oriented $PtN_2C_8H_{12}$ molecules, a net nonzero TRFR signal is obtained (presumed that all requirements for a TRFR experiment are satisfied). This implies that optically

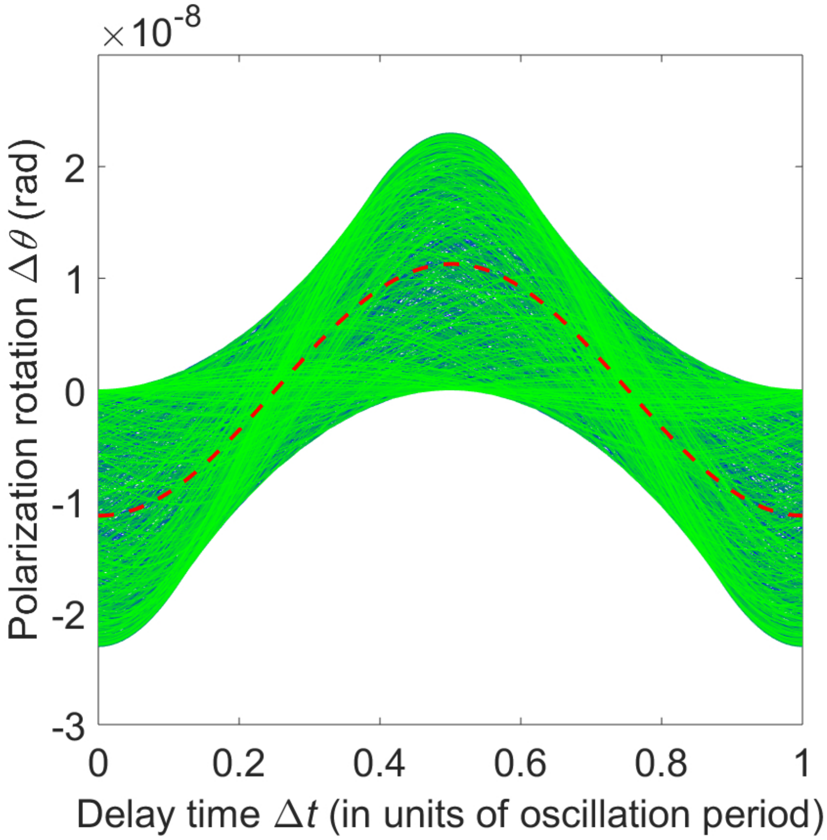

Figure 3.12: Calculation of $\Delta\theta(\Delta t)$ for the metal-organic molecule $\mathbf{PtN_2C_8H_{12}}$ (main text Fig. 3.1). Each line represents a different orientation of a sample with molecules all oriented similarly (where the color variation is merely intended for contrast). Besides, the only difference with respect to main text Fig. 3.4 is that a circular pump pulse is considered ($\hat{\mathbf{E}}_{pump} = \frac{-i\hat{\mathbf{z}}+\hat{\mathbf{y}}}{\sqrt{2}}$). Clearly, for an ensemble of randomly oriented $PtN_2C_8H_{12}$ molecules, a net TRFR signal is obtained. More specific, the total average TRFR signal (dashed line) for such an ensemble decreases with only a factor 2 with respect to an ensemble with all molecules oriented such that the maximum signal is obtained (i.e. perpendicular to the incoming light).

induced spin polarization can be applied to an ensemble of randomly oriented molecules.

To verify this conclusion with calculations, we study how $\Delta\theta(\Delta t)$ depends on the sample orientation with respect to the incoming pump and probe. We calculate $\Delta\theta(\Delta t)$ as in main text Fig. 3.4 for a sample consisting of similarly oriented $PtN_2C_8H_{12}$ molecules, with the only difference that a circular pump pulse is considered ($\hat{\mathbf{E}}_{pump} = \frac{-i\hat{\mathbf{z}}+\hat{\mathbf{y}}}{\sqrt{2}}$) and that the sample has a random orientation, obtained by using random values for the so-called proper Euler angles (which

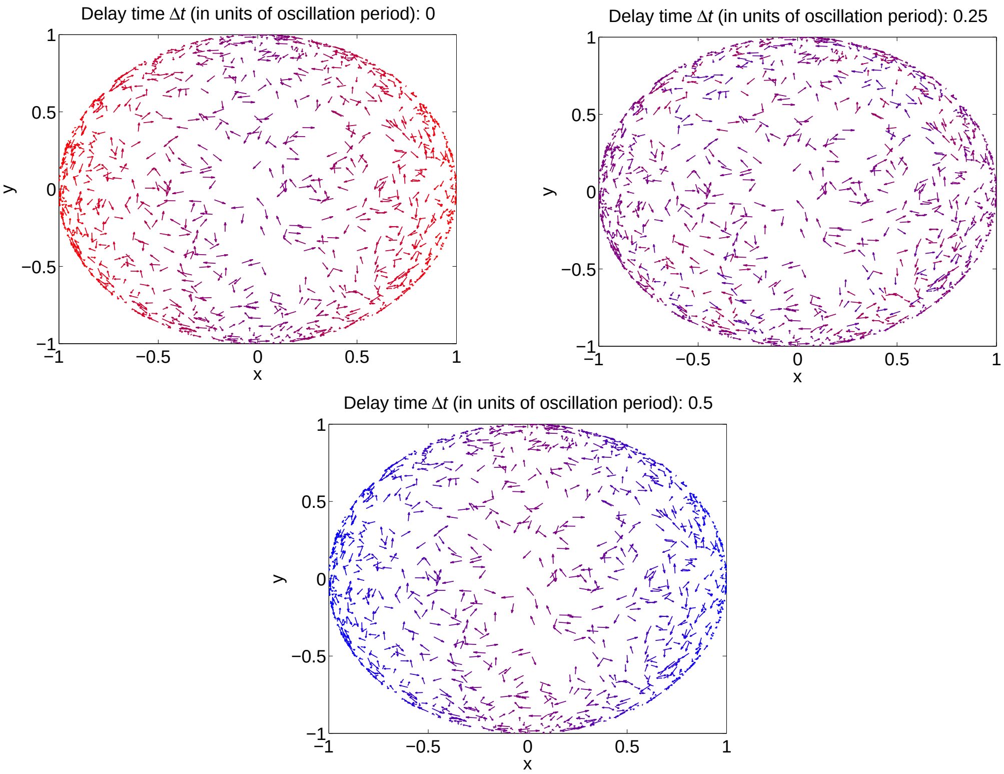

Figure 3.13: Visualization of the TRFR signal for different sample orientations (with the molecules in the sample oriented similarly) for the metal-organic molecule $PtN_2C_8H_{12}$ (main text Fig. 3.1). We consider a circular pump pulse ($\hat{\mathbf{E}}_{pump} = \frac{-i\hat{\mathbf{z}}+\hat{\mathbf{y}}}{\sqrt{2}}$) and three delay times, where for each plot the arrow corresponds to the value of a line in Fig. 3.12 at the corresponding delay time (i.e. each arrow represents a different orientation of a sample with molecules all oriented similarly). The color of the arrows correlates with the value of the TRFR signal at delay times Δt (in units of the oscillation period) equal to (a) 0, (b) 0.25, (c) 0.5. Each arrow is plotted tangent to the surface of a sphere which visualizes a sample orientation where the molecular $y''z''$ plane is parallel to the sphere and the arrow points in the z''-direction of the molecular frame (double primes denote the molecular frame transformed with respect to the lab frame, where randomly selected values are used for the so-called proper Euler angles). The incoming pump and probe pulse always propagate in the x-direction of the lab frame. We conclude that for an ensemble of randomly oriented molecules a nonzero TRFR signal is obtained.

can in general be used to describe the orientation of a rigid body). Each line in Fig. 3.12 represents a different orientation of a sample with molecules all oriented similarly (where the color variation is merely intended for contrast). The total average equals half the maximum signal (i.e. for a molecule oriented perpendicular to the incoming light), confirming our statement that for an ensemble of randomly oriented $PtN_2C_8H_{12}$ molecules, a net TRFR signal will be obtained. Note that a nonzero signal will also be obtained for a linear pump pulse, but this signal will be smaller.

Fig. 3.13 is a visualization of the orientation of the sample for each of the traces in Fig. 3.12. We consider three delay times, where for each plot the color (red: maximal negative, blue: maximal positive) of an arrow correlates to the value of a line in Fig. 3.12, at the corresponding delay time (each arrow represents a different orientation of a sample with molecules all oriented similarly). We consider delay times Δt (in units of the oscillation period) equal to (a) 0, (b) 0.25, (c) 0.5. For each case, an arrow pointing from the point (1,0,0) to the original z-direction (representing a molecule with its $y''z''$ plane perpendicular to the x-direction) is transformed using the same Euler angles used to transform the sample (we use double primes for the molecular frame to distinguish it from the lab frame). Accordingly, each arrow is plotted tangent to the surface of a sphere which visualizes a sample orientation where the molecular $y''z''$ plane is parallel to the sphere and the arrow points in the z''-direction. The incoming pump and probe pulse always propagate in the x-direction of the lab frame. Molecules having their $y''z''$ plane oriented parallel to the x-direction give zero TRFR signal at all delay times (visualized by the arrows at $x = 0$). Instead, molecules having their $y''z''$ plane oriented perpendicular to the x-direction give maximal TRFR signal when Δt equals a multiple of a half period of oscillation (visualized by the arrows at $x = \pm 1$). As it should, Fig. 3.13 confirms our statement that for an ensemble of randomly oriented $PtN_2C_8H_{12}$ molecules an oscillating TRFR signal is obtained with nonzero amplitude.

It is important to realize that the molecular tumbling motion might affect the TRFR experiment. In order to obtain a nonzero TRFR signal, it is required that the orientation of the molecules at the arrival of the pump is comparable to when the probe arrives. Following Berg[81], we take as a suitable measure for the tumbling motion the mean square angular deviation as a function of the elapsed time t

$$\left\langle \Theta^2 \right\rangle = 2D_r t \tag{3.80}$$

with the rotation diffusion coefficient given by

$$D_r = \frac{kT}{f_r} \tag{3.81}$$

with f_r the rotational frictional drag coefficient. For $PtN_2C_8H_{12}$, a rotation about an axis perpendicular to the face through the center does not affect the TRFR signal, such that we should consider a parallel axis. For a disk (radius a), rotating about an axis parallel to the face through the center, the drag constant amounts

$$f_{r,disk} = \frac{32}{3}\eta a^3 \tag{3.82}$$

with η the viscosity. It turns out that for a relatively small molecule like $PtN_2C_8H_{12}$ (we assume $a = 3.75$ Å), we need an extremely viscous host fluid to keep the tumbling motion small enough. Let us as an example consider glycerol, because of its exceptional range (10 orders of magnitude) of viscosities between its glass temperature ($T_g = 190$ K) and room temperature. Between 195 and 283 K, its viscosity η can be well estimated according to the Vogel-Fulcher-Tammann-Hesse law[82]

$$\eta = \eta_0 10^{\frac{B}{T-T_0}} \tag{3.83}$$

with $\eta_0 = 7.9 \times 10^{-8}$ Pa s, $B = 1260$ K and $T_0 = 118$ K. At 195 K, we have $\eta = 1.83 \times 10^9$ Pa s. Taking the square-root of Eq. 3.80 as a measure for the angular deviation at time t, we obtain the root-mean-square value $\sqrt{\langle \Theta^2 \rangle} \approx 32$ nrad for $t = 0.2$ ps (oscillation period of $\Delta\theta$ for $PtN_2C_8H_{12}$, main text Fig. 3.4), which is of the same order as the polarization rotation (up to 23 nrad, see Fig. 3.12 and main text Fig. 3.4) and will therefore strongly affect the signal. Hence, in order to perform a molecular TRFR experiment with a liquid host it would be better to take a larger molecule (such that the tumbling motion will be decreased), or one with a shorter oscillation period (such that the tumbling motion is on a longer time scale than the quantum dynamics). Probably, it is more practical to take a crystalline host, where (we have shown in this section that) the molecules of interest can have a random orientation.